Cometary Nuclear Magnitudes from Sky Survey Observations

Michael Weiler, Heike Rauer, Christiaan Sterken

HAL Id: hal-00725407
https://hal.science/hal-00725407

Accepted Manuscript

Cometary Nuclear Magnitudes from Sky Survey Observations

Michael Weiler, Heike Rauer, Christiaan Sterken

Please cite this article as: Weiler, M., Rauer, H., Sterken, C., Cometary Nuclear Magnitudes from Sky Survey Observations, *Icarus* (2010), doi: 10.1016/j.icarus.2010.12.026
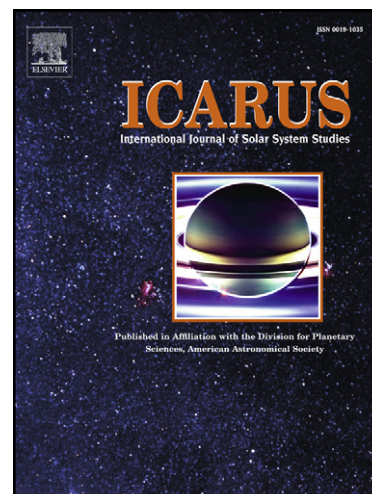
Cometary Nuclear Magnitudes from Sky Survey Observations

Michael Weiler [a], Heike Rauer [b,c] and Christiaan Sterken [d]

[a] GEPI – UMR CNRS 8111, Observatoire de Paris, Section de Meudon, 5 Place J. Janssen, 92195 Meudon

Cedex, France

[b] Institut für Planetenforschung, DLR, Rutherfordstrasse 2, 12489 Berlin, Germany

[c] Zentrum für Astronomie und Astrophysik, Technische Universität Berlin, 10623 Berlin, Germany

[d] Vrije Universiteit Brussel, Pleinlaan 2, B-1050 Brussels, Belgium

Pages: 48

Tables: 5

Figures: 8

1

Proposed Running Head: Cometary nuclear magnitudes from survey observations

Editorial correspondence to:

Michael Weiler

GEPI – UMR CNRS 8111

Observatoire de Paris, Section de Meudon

5 Place J. Janssen 92195 Meudon Cedex

France

Phone: +33 (0)1 45 07 78 44

Fax: +33 (0)1 45 07 78 78

E-mail address: michael.weiler@obspm.fr

Abstract

The determination of the nuclear magnitudes of comets, and with it nuclear size frequency distributions, is strongly complicated by cometary activity. By now, only nuclear size frequency distributions for Jupiter-Family comets are available, and they are still subject of uncertainties. For comets of other dynamical classes, nuclear magnitudes are known for only a few comets. The size frequency distributions are thus not well constrained.

In this work we study whether nuclear magnitudes of comets can be constrained from sky survey observations as published by the Minor Planet Center. Observations from sky survey programs in which the comet was classified as a point-like source are analyzed in this respect.

From the available published observations from 1998 to 2008, we derive nuclear magnitudes, as well as nuclear radii, for 84 comets. Among these are comets of the Jupiter Family, dynamically old and new isotropic comets, Halley-type comets and Centaurs. For Jupiter Family comets and for isotropic comets, the size frequency distributions are presented.

Uncertainties of derived nuclear magnitudes arise from photometry and from potentially undetected activity. However, a comparison with objects with well known nuclear parameters shows that, despite substantial observational uncertainties, nuclear magnitudes are constrained to ± 0.6 mag, thereby providing first indications for nuclear sizes. This is particularly relevant for isotropic comets with so far ill-constrained size distributions. Exponents of the differential size frequency distributions of $2.01^{+0.21}_{-0.17}$ for Jupiter Family comets and $1.56^{+0.15}_{-0.12}$ for isotropic comets are presented. The values derived here form a basis for future, dedicated observational studies which provide higher measurement accuracy.

Key Words: Comets, nucleus

1 Introduction

1.1 Motivation

Size frequency distributions of small bodies in the Solar System are a source of information on the history of the Solar System and of the properties of its constituents. Effects like collisional processing of a population of objects, and the internal strength of the objects, influence the size frequency distribution (Bagatin 2006). Furthermore, the size frequency distributions are of importance for estimating the amount of material that was delivered to terrestrial planets by impacts of minor bodies. Such delivery is of particular interest if organic matter or water is concerned. Comets are of special interest in this respect, since they are known to contain significant amounts of both substances (Despois et al. 2005). Furthermore, since isotropic comets are believed to have been stored in the low-density Oort Cloud over most of the lifetime of the Solar System, their size frequency distribution probably is the closest to the one of the planetesimals of the early Solar System. The study of the sizes of cometary nuclei is therefore of particular interest.

1.2 Overview of nuclear magnitude determination methods

From the observed magnitude of a planetary body in the Solar System and the known heliocentric and geocentric distance (r_h and Δ, respectively), the reduced magnitude (i.e. the magnitude normalized to 1 AU of heliocentric and geocentric distance at a phase angle β), $H(1, 1, \beta)$ can be determined. Together with the geometric albedo (p_v), phase angle, and phase function, the radius of the object can be computed. For cometary nuclei, this method for the determination of the sizes is strongly complicated by the appearance of cometary activity. When approaching the Sun, increasing irradiation results in the sublimation of volatiles on or near the surface of the cometary nucleus. The volatiles, expanding into space and carrying dust particles with them, cause the formation of an extended, diffuse coma. Light emission from radicals formed in this coma, as well as sunlight scattered by the dust particles, contribute to optical observations of the nucleus, and it becomes a demanding task to separate the light reflected off the nucleus from the coma contributions. Two methods are applied to solve this difficulty.

The first is the observation of cometary nuclei at large heliocentric, and thus geocentric, distances. At large distances, the solar irradiation is too low for significant sublimation of material on the nucleus. However, isotropic comets seem to remain active up to very large distances from the Sun (e.g. Comet C/1995 O1 Hale-Bopp is still observed to be active at $r_h \sim 26$ AU (Szabó et al. 2008)). Thus, this method was successfully applied only to comets of the Jupiter Family, appearing as point-like sources and thus probably inactive at their aphelia at about 5 to 6 AU from the Sun.

The second method is the modeling and subtraction of the dust coma brightness from images of the

4

comets, obtained at wavelengths where emissions by gaseous species can be neglected (Lamy et al. 2004). This method requires images with very high spatial resolution to obtain sufficiently high contrast between the nucleus and the coma signal, as well as an approximately symmetric dust coma. Therefore, this method remains restricted to a relatively small number of comets.

Furthermore, in addition to the methods mentioned, two completely different approaches for the determination of cometary nuclear sizes can be chosen. One is the active radar detection of the nuclei during a close passage to Earth. Since the intensity of the received radar signal after reflection from the nucleus decreases with the geocentric distance Δ to the power of minus four, this method is limited to a very small number of comets, coming sufficiently close to Earth. The most precise method is to take resolved images of the nucleus within the frame of a space mission to a comet. This method is again limited to a very small number of comets as it is very expensive in resources. It is due to these circumstances that up to date the number of comets for which reliable nuclear radii are available is rather small. Four comets (three of the Jupiter Family and comet Halley) were imaged from spacecraft. Furthermore, for about one hundred comets of the Jupiter Family, nuclear radii were obtained by the other methods described above. The nuclear size frequency distribution of the Jupiter Family was derived by different authors (e.g. Meech et al. (2004), Tancredi et al. (2006), Whitman et al. (2006)), but the results are not in satisfactory agreement. For isotropic comets, estimates of the nuclear sizes are only available for a few objects, together with upper limits in size for some additional comets. The size frequency distribution for this class of comets is therefore unknown.

1.3   Approach of this work

During the last years observations of comets have come up with more and more indications that some comets are also not continuously active on their orbital arc in the inner Solar System, under significant solar irradiation. This was shown for Comet C/2001 OG$_{108}$ (Abell et al. 2005) and 133P/Elst-Pizarro (Jewitt et al. 2007). For comet C/2001 OG$_{108}$ the presence of a period of activity is illustrated in Fig. 1, showing the reduced magnitudes versus time. All available magnitude estimates provided by the MPC extended computer service are used in this Figure. The increase in brightness shifted towards the perihelion date indicates periodic activity. This raises the question whether the nuclear magnitude of comets can be determined from inner Solar System data while they are in a temporary state of inactivity.

During the last decade the majority of comets were discovered by large sky survey programs designed to discover near-Earth objects and to determine their orbits. These programs, such as LINEAR (*Lincoln Near-Earth object Research*, Stokes et al. (2000)), NEAT (*Near-Earth Asteroid Tracking*, Helin et al. (2000)), LONEOS (*Lowell Observatory Near-Earth Object Search*, Koehn & Bowell (2000)) observe large areas of the sky towards the opposition direction and provide in addition to astrometric data also a crude magnitude

estimate and information of the appearance of an object as extended or point-like. After discovery of a comet by such a program, often some follow-up observations are published for astrometry and confirmation on the cometary appearance of the object. It turns out that about one third of the newly discovered comets were classified as point-like objects at the time of their discovery. Structures like comae or tails that confirm the cometary nature of the objects are discovered at a later time. In this work, such observations of apparently point-like comets will be used to derive estimates of the nuclear magnitudes.

2 Observational bases

2.1 Observational data set

For this work, all comet discoveries from the years 1998 to 2008 are analyzed to identify comets that were at the time of their discovery classified as point-like. As the basis of this work, the observations of comets published by the Minor Planet Center Extended Computer Service were used. We restrict the study here to comets that where inactive at their time of discovery, and thus exclude the possibility that a once active comet could become inactive again. This restriction was chosen to minimize the influence of undetected activity. If a coma has been observed at one time, there will be the possibility that some undetected coma still contaminates the observations at later times when the object is regarded inactive.

In the past, magnitudes from the Minor Planet Center have been used to determine nuclear magnitudes of comets (Tancredi et al. 2000, Tancredi et al. 2006), provoking critique concerning the reliability of the magnitude estimates (see e.g. the discussion in Tancredi et al. 2006). Therefore, in this work only magnitudes derived from CCD observations of comets were taken into consideration. Furthermore, these data must allow for a quantitative evaluation of the accuracy. This evaluation is described in the following section.

2.2 Photometric analysis

For the determination of nuclear magnitudes, the accuracy of the available magnitude estimates has to be evaluated. To exclude the influence of potential cometary activity in such an evaluation, observations of asteroids were used instead of comet observations. Although this study cannot provide a full calibration of the observations and methods used, it gives an indication for the photometric errors of the magnitudes provided by different observers and surveys. For the selection of suitable asteroids, several constraints have to be considered.

The color of cometary nuclei is only known for a small number of comets, and the mean color $V - R$ is 0.41 (Lamy et al. 2004). It is not clear whether these colors are representative for all comets studied in this

work. To include the uncertainties in magnitude introduced by possible differences in color, the color of the asteroids used for this accuracy study should therefore cover a broad range. Furthermore, the known shapes of cometary nuclei range from roughly spherical (e.g. Comet Wild 2, Kirk et al. (2005)) to very elongated (e.g. comet Borrelly, Oberst et al. (2004)). To include the influence of rotational variation in the study of the photometric accuracy, asteroids with various amplitudes in the rotational light curve should be included. In order to meet these constraints, observations of asteroids of different types were treated in the following, including near-Earth objects, Mainbelt asteroids, and Trans-Neptunian objects. The mean $V - R$ color of Main-Belt asteroids, estimated from 22 objects (Piironen 1998) is 0.42, while Trans-Neptunian objects have a mean $V - R$ of 0.61 (Jewitt 2002). Therefore we do not expect to introduce a systematic photometric error by using a sample of these objects. In total 1113 observations of 206 different asteroids were analyzed. Since a significant number of observations of different objects have to be available in this study, we are restricted to 14 observers providing the largest amount of magnitude estimates. These observers are identified by their 3-digit observatory code in Table 1.

We discuss three different aspects of the photometric accuracy. First, the variations in magnitude of each particular object observed by an observer within a certain night is studied. This analysis allows us to constrain the stability of the instrument, the variation of sky transparency during the night, the influence of changing extinction during the night, and the variation of brightness due to rotation of the object. As typically the number of magnitude estimates for a comet observation is not sufficient to estimate this uncertainty for each night individually, we computed the average uncertainty from a number of asteroid observations. For this purpose we selected nights in which at least five magnitude estimates for a particular asteroid are provided by an observer. From this data we computed the standard deviation for each individual night. This value varies from night to night, so from the results for a number of individual nights we used the mean standard deviation as the average uncertainty of one observer. The results obtained for different observers were found to be similar, so in the following we simply apply the typical value of $0.^{\mathrm{m}}30$ as the typical uncertainty of a single observer.

Second, the differences in magnitude estimates of an object provided by different observers for the same time of observation were evaluated, which allows us to constrain systematic biases between different observers. Such biases could be caused by different photometric bandpasses or different methods applied to derive the magnitude. Since strictly simultaneous observations by different observers are not available, the condition "at the same time" means here that the observing geometry, i.e. the heliocentric and geocentric distance and the phase angle, did not significantly change within the times of different observations. The times between different observations for one object thus range from less than one hour for near-Earth objects up to 26 hours for Trans-Neptunian objects. All observations of one object by one observer were averaged before comparing with nearly−simultaneous observations by other observers. The differences

7

between these averaged magnitudes were computed, and from a number of such differences for different objects and different nights the mean bias and its standard deviation was computed. The derived biases between the different observers are presented in Table 1.

[Table 1]

As reference, the observer providing the largest number of observations was selected. This observer provides photometry in the *R*-band. It can be seen that, except for one observer, the results are in agreement. Nevertheless, the presented biases were subtracted from the magnitude estimates for further analysis to normalize all observations to a single observer. The typical uncertainty in the bias for the different observers was estimated to $0\overset{\text{m}}{.}50$.

From these two aspects of analysis, the total photometric uncertainty for these selected observers is assumed to be the quadratic sum of the two individual uncertainties, i.e. $0\overset{\text{m}}{.}58$. This value is slightly larger than the scatter of photometric data found for asteroids in the Sloan Digital Sky Survey data set (Jurić et al. 2002), which can be explained by the inhomogeneous data base used in our work.

Third, the magnitude estimates normalized to one observer for well known objects were compared to expected magnitudes computed from the physical parameters and ephemeris of these objects. This third step in the analysis allows us to check whether the estimation of the uncertainty in the magnitude estimates as described before is reasonable. Furthermore, the absolute accuracy of the magnitude estimates can be checked by comparing with well-known reference objects. As reference objects the four asteroids 243 Ida, 253 Mathilde, 433 Eros, and 951 Gaspra were chosen, since these objects have been well observed by the different observers which are of importance in this study. Furthermore, the sizes, albedos, and phase functions of these two bodies are well known from spacecraft flybys (Clark et al. (2002) for Eros, Clark et al. (1999) for Mathilde, Thomas et al. (1996) for Ida, and Thomas et al. (1994) for Gaspra). Theoretical magnitudes of these four asteroids were computed based on the values of albedo and phase function for the times at which the objects were observed from ground. The difference between this theoretical magnitude and the measured magnitude is presented as a function of phase angle in Fig. 2. The mean and the estimated uncertainty for the magnitudes is also shown. When regarding the scatter of the individual data points for the four asteroids in Fig. 2, it turns out that our estimate of $0\overset{\text{m}}{.}58$ for the uncertainty of an individual data point is reasonable. Furthermore, within the estimated photometric uncertainty, the observed magnitudes of the four asteroids are in agreement with the theoretical expectations. We note that the deviation between the theoretical and measured magnitudes for Eros is larger than for the other asteroids. This is most likely caused by the higher asymmetry of the shape of this asteroid, resulting in a higher amplitude in its lightcurve. For all asteroids in Fig. 2, the mean for all data points lies at a similar value below zero. Such a systematic bias can be caused by the fact that the photometry was not normalized to a standard *R*−filter bandpass. In

the following analysis, we correct for the mean bias obtained from all four asteroids, which is –0$^{\text{m}}$28.

[Figure 2]

2.3   Selection of inactive comets

To derive nuclear magnitudes, first obviously wrong classifications as point-like have to be rejected and good candidate comets have to be selected. It is possible that comets were classified as point-like objects and thus as potentially inactive although activity was present. This is suggested by additional observations made by the same or other observers shortly after the original observation and revealing cometary activity. Such erroneous classifications could be caused by poor seeing, a low limiting magnitude given by the telescope/detector or the sky conditions, etc. In order to reject comets that were obviously wrongly classified as point-like from the further analysis, two selection criteria were applied to all observations of comets discovered from 1998 to 2008.

First, for a comet to be included in the further analysis, a minimum time between the discovery of the object and the discovery of its activity is required. Fig. 3 illustrates this time interval for all comet discoveries from 1998 to 2008. In this diagram, the cumulative number of comets with observed activity is shown versus the time between the discovery of the comet and the first observation of activity. This time period ranges from the next following night up to several years. When a cometary coma is observed within a few nights after the classification as point-like, this classification was probably wrong. However, a long time interval between the observation of a point-like object and cometary activity raises the question whether for a number of comets inactivity or at least insignificant activity can be assumed for some observations. The time interval was set to 10 days in this work for including a comet in the further analysis. This value was chosen since it has to be in principle possible for an object to build up a cometary coma between the observations of a point-like object and the first observation as an active object. When regarding the reports on the discoveries of activity, the coma diameter is typically less than about 25″ when recognized. Since the most distant comets regarded are at about 10 AU from the Earth at time of discovery, and further assuming a nucleocentric dust expansion velocity of 0.1 km s^{-1}, a dust coma with a diameter of 25″ can be build up from an inactive state for all investigated objects within the selected period of time.

Furthermore, at least two independent observations confirming the point-like appearance of an object are required. Independent means made by two different observers or by one observer, but in different nights. This condition is introduced to reduce the dependency on the observing circumstances of a single night. Also pre-discovery observations are considered, and comets are included in the data set of this work if the two conditions above are satisfied by pre-discovery observations.

When applying the two selection criteria described in this section to exclude active objects from further

9

analysis, and regarding only observations by the 14 observers listed in Table 1, 84 comets remain in the data set analyzed further in this work. Among these objects are 46 Jupiter Family comets, 3 comets of Halley type, one Centaur, 18 dynamically new, and 16 dynamically old comets (applying the classification scheme by Levison (1996)). Table 2 provides an overview on the basic parameters of these comets.

[Table 2]

[Figure 3]

2.4 Influence of undetected activity

The selection criteria described in section 2.3 were applied to reject objects with obviously wrong classifications as point-like sources. However, to estimate the degree to which the presented nuclear magnitudes and radii are affected by undetected or unrecognized activity, further tests are desirable. Two possible ways allow us to constrain the amount of light from the cometary coma that is polluting the nucleus signal. The first method is the analysis of the point-spread function of the observed object. Is the point-spread function broader than the one of a star, cometary activity is obvious. However, for the majority of observations analyzed in this work, no detailed information on the point-spread functions is available.

Another approach makes use of photometric measurements of an object at different heliocentric distances. For an inactive object, its brightness varies with the heliocentric and geocentric distance to the power of minus two. If an object shows cometary activity, the activity itself also scales with the heliocentric distance, since the sublimation of volatiles is triggered by solar irradiation. Therefore, the brightness of an active object is expected to depend stronger on r_h than on a power of minus two. If photometric observations covering a wider range of heliocentric distances are available, these observations can be used to check whether the long-term lightcurve is in agreement with an inactive object. It is therefore of interest to study the lightcurves of the comets in our data set.

As we have a large number of comets in our data set, the lightcurves have to be rendered in a normalized way to present them all in one graph. Therefore, we show only the difference between the absolute magnitude in Table 3 and the absolute magnitude derived from each individual data point instead of the true absolute magnitude which covers a broad range of values for the different comets. Furthermore, we do not plot this difference versus the true heliocentric distance, as r_h also covers a broad range for the different comets. Instead, we plot it versus the relative change in heliocentric distance with respect to the heliocentric distance at which activity was first detected, $r_h(active)$, i.e. $r_h/r_h(active)$. This approach is justified as the relative change in heliocentric distance is likely to have significant impact upon the changes in the lightcurve, and not the absolute values of r_h. The variation of brightness with changing heliocentric distance for all comets in the data set is shown in Fig. 4. In this Figure, changes in r_h with respect to $r_h(active)$ are

10

plotted to the right hand side if it corresponds to observations of a comet in active state, and to the left hand side if the observation was done while the object was still regarded as inactive. A value of, e.g. two for the relative change in heliocentric distance on the left hand side of Fig. 4 thus can mean an observation of the inactive object made at a heliocentric distance being a factor of two different from the r_h at the time activity was discovered. A point on the right hand side would belong to an observation of the object after its activity was detected and at a heliocentric distance different by a factor of two. As the activity of some objects was detected on the inward branch of their orbits, for other objects while on their outward branch, the factor of two can either mean double or half in heliocentric distance with respect to $r_h(active)$. Data points from observations when activity of the object was confirmed are included in this Figure for comparison only. None of the data points from active comets were included in the photometric analysis of this work.

There is no significant systematic variation of the absolute magnitude with relative heliocentric distance for any comet in our data set. However, for most objects the relative change in heliocentric distance is too small to expect a significant change in brightness due to activity, taking into consideration the large photometric uncertainty. Only for a few objects, the relative change in r_h is so large that we can exclude any activity. The data points belonging to one of these comets, 162P, are highlighted in Fig. 4. Here r_h changes almost by a factor of four, while no systematic deviation from a constant absolute magnitude is observed.

As one easily sees from Fig. 4, the scatter of the data points for active comets is much larger than for inactive comets. An increase relative to the inactive state would be expected due to the increasing activity. However, the data points scatter in both directions. This is illustrated for one comet, C/2002 T7, whose data points are highlighted. This comet developed strong and obvious activity, but the brightness tends to decrease below the brightness of the inactive object. It is likely that the determination of the brightness of a comet becomes less accurate as the PSF of the comets becomes different from that of a star. The scatter in both directions can be explained by such effect.

For some comets in the data set, photometric measurements at only one heliocentric distance are available while the object is supposed to be inactive. However, such comets could display a steep and systematic increase in brightness when activity was recognized. Data points for one comet of this type, P/2002 T6, are highlighted in Fig. 4. For such comets it remains highly uncertain whether it was active or inactive at the time classified as point-like.

As shown in section 3.1, all large nuclei in the data set were observed at large geocentric distances. At large distances, the spatial resolution of the observations and the apparent brightness is low, and activity could more easily remain undetected, which results in overestimated nuclear sizes. Therefore it has to be evaluated what cometary activity could remain undetected at such large discances and thus low spatial resolution. In order to estimate the order of magnitude of undetected activity that would falsely result in the larger nuclear radii of isotropic comets compared to the sizes of Jupiter Family comets, we estimate the

11

activity, expressed in terms of Afρ, that would result in the observed largest radius of an isotropic comet, assuming that its true radius is the same as for the largest Jupiter Family comet in our data set. Thus we assume an isotropic comet of 15.5 km in radius (the largest one in the data set of this work, see section 3.1) to be at 10 AU heliocentric and 9 AU geocentric distance and determine the Afρ value that would provide sufficient flux to result in a nuclear radius of 76.1 km (the largest radius for a long period comet in our data set, see section 3.1), if remaining unrecognized. This Afρ value can be compared with the values in other comets for which activity is easily discovered. To do so, we assume a spherically symmetric coma where the brightness decreases with the projected nucleocentric distance ρ according to ρ^{-1}. Furthermore, we assume that the flux of the object was integrated over a seeing disc with a 3-σ aperture (σ being the standard deviation of a Gaussian PSF), while the seeing was 2″ (FWHM). With these assumptions, the dust coma has to contribute 23.2 times the flux of the nucleus. This corresponds to an Afρ value of 5215 cm. This value corresponds to the dust activity of comet 1P/Halley at about 1.4 AU heliocentric distance (Fink 1994). It is therefore unlikely that such a large dust activity can remain unrecognized for several observations. This supports the view that the nuclei of isotropic comets indeed extend to larger radii than Jupiter Family comet nuclei, as discussed in section 4.4.

[Figure 4]

3 Absolute nuclear magnitudes and radii

3.1 Determination of nuclear magnitudes and radii

From the observed magnitude $m(r_h, \Delta, \beta)$, the reduced magnitude $H(1, 1, \beta)$ can be obtained by applying the relation:

$$H(1, 1, \beta) = m - 5 \log(r_h) - 5 \log(\Delta) \quad . \tag{1}$$

For the correction of the phase angle β at the time of observation to a phase angle of zero, and thus to obtain the absolute magnitude, a phase function has to be applied. For cometary nuclei, only limited information on the phase function is available. In this work, the IAU-adopted H, G-phase law (Bowell et al. 1989) is used. This law is able to reproduce the observed phase function of Comet 28P/Neujmin 1 (Delahodde et al. 2001). The correction for the phase angle has the form

$$H(1, 1, 0) = H(1, 1, \beta) + 2.5 \log \left[(1 - G) \exp \left\{ -3.33 \tan^{0.63}(\beta/2) \right\} + G \exp \left\{ -1.87 \tan^{1.22}(\beta/2) \right\} \right] \quad . \tag{2}$$

The parameter $G = 0.41$ is taken from Delahodde et al. (2001). With this parameter, the phase law can fit the observed phase function of Comet 28P/Neujmin 1 between phase angles 0°.7 and 17°.7. The range of

12

phase angles covered by observations analyzed in this work range from $0°.1$ up to about $60°$. However, for objects for which phase functions were derived over a broader range of phase angles, it turned out that the slope remains about constant up to $60°$, e.g. for Mathilde (Clark et al. 1999), Eros (Clark et al. 2002), and Mercury (Mallama et al. 2002). Therefore, the assumption of the given phase law for phase angles up to $60°$ is justified. For small phase angles between $0°.7$ and $0°.1$ it is assumed that the (H,G) phase law describes the expected increase in brightness.

From $H(1, 1, 0)$ the nuclear radius R_N (given in meter) is obtained according to (Russell 1916):

$$R_N = \sqrt{2.2 \cdot 10^{22}/p_v \cdot 10^{0.4(m_\odot - H(1,1,0))}} \quad ; \tag{3}$$

where $m_\odot$ represents the solar magnitude in the photometric bandpass and p_v represents the geometric albedo of the cometary nucleus. A value of $-27^m.13$ for R-band is applied here. This quantity could be derived for a number of cometary nuclei. The values range typically from 0.02 to 0.05 (Lamy et al. 2004). Here, the widely used value of 0.04, derived for the nucleus of comet Halley and similar to the nuclear albedo of other comets, is assumed. The nuclear magnitudes and the derived nuclear radii for the comets in the database are presented in Table 3. From the estimated photometric uncertainty of $0^m.58$, it follows from equation 3 that the uncertainty in the nuclear radius is 27%.

[Table 3]

3.2 Comparison with the results of independent studies

For some of the comets in the data set analyzed in this work, independent studies of the nuclear properties are available. These studies are based on detailed observations of few particular objects and thus allow us to test the reliability of the presented method in the particular cases discussed in the following.

Comet C/2001 OG$_{108}$. For this comet, a nuclear radius of (7.5 ± 2.0) km was determined in this work. Abell et al. (2005) present a detailed study of this object, including optical and thermal infrared observations. These observations were done at a time when the absence of a cometary coma was confirmed by imaging. The geometric albedo of 0.04 assumed for all bodies in this work was confirmed for that object. The effective nuclear radius given by Abell et al. (2005) is (7.6 ± 1.0) km. The results are therefore in good agreement.

Comet C/2002 VQ$_{94}$. In this work, an absolute nuclear R-band magnitude of $8^m.65 \pm 0^m.58$ was determined. Jewitt (2005) presents a corresponding value of $9^m.22 \pm 0^m.02$, thus slightly larger than the value derived here, but still in agreement within the error bars. However, Jewitt (2005) applied a linear phase law with 0.04 mag/degree, which is different from the phase law assumed in this work. Using the same phase function as Jewitt (2005), the value of $8^m.74 \pm 0^m.58$ results in this work, in agreement with the result by

Jewitt (2005). The confirmation of the nuclear magnitude of this object is of particular interest, since it confirms the existence of very large cometary nuclei. It has to be noted that comet C/2002 VQ$_{94}$ was displaying a coma in the observations by Jewitt (2005), but the contribution of the coma to the nuclear signal was estimated to be below 20%.

Comet 162P/Siding Spring. In this work, a nuclear radius of (5.0 ± 1.4) km was derived. Fernández et al. (2006) studied this object in the optical and thermal infrared at a time when no cometary activity could be detected. They present a geometric R-band albedo of (0.037 ± 0.014) for this object, thus in agreement with the assumptions made here. The effective radius was found to be (6.0 ± 0.8) km, in agreement with the result of this work.

Comet P/2006 HR$_{30}$. This comet was studied in detail by Hicks & Bauer (2007). They present an absolute R-band magnitude of $11\overset{\mathrm{m}}{.}99 \pm 0\overset{\mathrm{m}}{.}01$, while the value derived in this work is $12\overset{\mathrm{m}}{.}19 \pm 0\overset{\mathrm{m}}{.}58$. Thus both values are in agreement.

Comet 172P/Yeung. Tancredi et al. (2006) give an estimate of the nuclear magnitude of this comet of $15\overset{\mathrm{m}}{.}0$. However, this estimate belongs to the lowest quality class in their work, having an uncertainty between $1\overset{\mathrm{m}}{.}0$ and $1\overset{\mathrm{m}}{.}5$. In our paper, the absolute magnitude of this object was estimated to $14\overset{\mathrm{m}}{.}10 \pm 0\overset{\mathrm{m}}{.}58$. Thus, the two results are in agreement within their very large error bars.

Comets P/2001 TU$_{80}$, P/2001 YX$_{127}$, P/2002 JN$_{16}$, and P/2002 T6. For these four comets, Hicks et al. (2007) present nuclear diameters derived from an analysis of NEAT observations. These authors used a value of 0.05 for the albedo. When correcting their resulting radii to the value of 0.04 used in our work, one obtains for the four comets the radii of (2.0 ± 0.1) km, (3.6 ± 0.4) km, (1.8 ± 0.1) km, and (4.6 ± 0.4) km, respectively. The values derived in the present work are (3.2 ± 0.9) km, (4.8 ± 1.3) km, (1.9 ± 0.5) km, and (4.2 ± 1.1) km. The results for the last three comets are thus in good agreement. For the first of these comets, our result is slightly higher than the one presented by Hicks et al. (2007). However, we do not know what correction for the phase angle was applied in deriving the nuclear radii by these authors. The one comet for which a larger size was derived in our work was also the one among the four comets observed at largest phase angles. Part of the deviation between the two estimates of the nuclear size could therefore be caused by different assumptions on the phase law.

Detailed studies of nine comets from our data set were published by other authors. For eight of these, a satisfying agreement between the different results was obtained. For the ninth comet, the size determined in this work is slightly higher than published before. However, all comets for which a comparison with independent studies were possible are dynamically evolved. No confirmation of the derived nuclear magnitudes for dynamically new comets is possible by now.

4 Magnitude and size frequency distributions

4.1 Determination of the power law exponents for sparse and noisy data

Fitting of power laws to data with observational error was discussed by Koen & Kondlo (2009) for the case of normal distributed noise with constant standard deviation σ[1]. In the following we describe a procedure to fit a power law to noisy data, including the option that the standard deviation of the normal distributed noise is a function of the noiseless observational quantity. For the determination of the slope of the size frequency distribution we assume that the true radius of any observed comet obeys a power law distribution, which holds on a finite size interval $[r_{min}, r_{max}]$. Thus the probability for detecting a comet having the nuclear radius r, $\hat{p}(r)$, is given by

$$\hat{p}(r) = \frac{1 - \alpha}{r_{max}^{1-\alpha} - r_{min}^{1-\alpha}} \, r^{-\alpha} \tag{4}$$

inside the interval $[r_{min}, r_{max}]$, and zero otherwise. Furthermore, we add observational noise x to the true radius of the comet, assuming a normal distribution for x, $\tilde{p}(x)$, with the standard deviation equal to our estimate of the observational uncertainty, i.e. 27% of the nuclear radius. The joint probability for obtaining an observed radius $\bar{r} = r + x$, $p(\bar{r})$, is then the product of $\hat{p}(r)$ and $\tilde{p}(x)$:

$$p(r, x) = \hat{p}(r) \times \tilde{p}(x) \, . \tag{5}$$

The probability density for the observed radius $\bar{r}$ is then obtained according to (Grimmett & Welsh 1986):

$$p(\bar{r}) = \int_{-\infty}^{\infty} p(r, \bar{r} - r) \, \mathrm{d}r \, , \tag{6}$$

which results in

$$p(\bar{r}) = \int_{r_{min}}^{r_{max}} \frac{1 - \alpha}{r_{max}^{1-\alpha} - r_{min}^{1-\alpha}} \, r^{-\alpha} \, \frac{1}{\sqrt{2\pi}\sigma(r)} \exp\left\{ -\frac{1}{2} \frac{(\bar{r} - r)^2}{\sigma^2} \right\} \, \mathrm{d}r \, . \tag{7}$$

From that expression, we obtain the likelihood for any observational data set with n comets, given the size interval and the power law exponent α:

$$L = \sum_{i=1}^{n} \ln\left(p(\bar{r}_i)\right) \, , \tag{8}$$

were i runs over all comets in the data set. In case of sparse data, the upper limit of the size interval within which a power law holds is poorly constrained. Therefore, we assume r_{max} to be much larger than the largest nuclear radius in our data set, i.e. $r_{max} \to \infty$. Thus, we have to maximize the expression for L with respect to the lower limit of the size interval, r_{min}, and the power law exponent α. By doing so, we are able to obtain an unbiased value for α even with sparse data affected by considerable noise. **It should be noted that r_{min}**

---

[1]The existence of this paper was only discovered during the revision phase of this manuscript.

only represents the lower limit to which the power law extends. So although for all data points i**,** $r_i > r_{min}$**, due to the normally distributed noise contribution, an observed radius** $\bar{r}_i$ **in the data set can be smaller than** r_{min}**.**

For the maximization of L, we used a downhill-simplex algorithm. To avoid trapping in local maxima, we used a re-initialization strategy for the simplex (Press et al. 2007) and applied different initial guesses for the parameters r_{min} and α. In all cases we converged quickly to only one maximum, L_{max}. The integral expression in equation (7) was computed using a Romberg integration scheme.

Appendix A presents tests of the presented scheme for the determination of the parameters α of a sparse and noisy power law distribution. Its performance is also compared with the performance of schemes not taking noise into account, such as the one presented by Newman (2005). For these tests, artificial random data is used.

In order to obtain the 1σ-confidence intervals for α, we used the condition that at the boundaries of that confidence region the condition $L_{limit} = L_{max} - 1/2$ holds (Lyons, 1986). The errors in different directions from the best fit value of α were determined separately, resulting in asymmetric errors. As the errors of r_{min} and α are correlated, we used an iterative scheme for the marginalization.

It now has to be validated that our model, i.e. the assumption that the nuclear radii in our data sets for the two comet populations are drawn from a power law with our best-fitting parameters and an additive normal noise with $\sigma = 27\%$ of the nuclear radius, is statistically in agreement with our data. To test this, the probability for obtaining a maximum likelihood less than our best-fit likelihood L_{max} under our assumptions has to be computed. If this probability is close to zero, the model fails to reproduce the observational data. If it is close to one, the model reproduces the data too well to be trustworthy. The distribution of the likelihood L was computed numerically. For this purpose, 100 sets of artificial data sets for the Jupiter Family comets and the isotropic comets were computed, respectively. For these test data sets, the best fitting parameters, the same number of data points, and the same assumption on the observational noise as in our real data were applied. From these different sets of artificial data we can determine the fraction that has a likelihood L less than L_{max} of our real data sets and use these fractions as a measure for the probability of obtaining a data set with $L < L_{max}$.

Furthermore, a Kolmogorov-Smirnov test (KS-test) was performed. This statistical test is not sensitive to the total deviation between the data set and the assumed probability density distribution, but to the the maximum deviation by an individual data point in the cumulative size frequency distribution of the data and the one of the assumed probability distribution. We were following the procedure described by Press et al. (2007) when performing the KS-test with the data sets of Jupiter Family comets and isotropic comets and their best-fitting distributions, respectively.

16

4.2 Determination of magnitude and size frequency distributions

For the study of the distributions of nuclear magnitudes and nuclear radii, the comets in the data set of this work are divided into two groups, the Jupiter Family comets, that make one large dynamical group in the presented data set, and the isotropic comets. The latter group includes the dynamically new and old isotropic comets, as well as the Halley-type comets. This division was chosen since the two groups probably have different dynamical histories. The Jupiter-family comets are assumed to have undergone a larger number of perihelion passages in the inner Solar System than the dynamically new isotropic comets. Thus they might be affected stronger by processes that potentially alter the size frequency distributions (e.g. cometary activity, splitting). Furthermore, the source regions of the two groups are most likely different. While the Jupiter-family comets mainly originate from the Transneptunian region, the isotropic comets enter the inner Solar System from the Oort Cloud. In these source regions, the comets might have been collisionally processed to different degrees. It is therefore of interest to study whether any differences in the frequency distributions between the two groups can be identified, and to correlate them with the history of the objects in the source regions. Because of its different dynamical history, the only Centaur in our data set is not taken into consideration in the size frequency distributions determination.

Fig. 5 shows the distribution of the derived absolute magnitudes for the two different groups of comets. From the nuclear radii presented in Table 3, the slopes of the size frequency distributions of the Jupiter Family comets and the isotropic comets can be determined. However, this is complicated by the small number of comets in our data set, and the large uncertainty in the absolute magnitudes. To be able to obtain meaningful results on the size distribution slopes, we chose the maximum likelihood method outlined in the previous paragraph. We obtained the value of $2.01^{+0.21}_{-0.17}$ for the power law exponent of the Jupiter Family population. For the isotropic comets, we found the exponent of $1.56^{+0.15}_{-0.12}$. Thus, in our data set the size frequency distribution of the isotropic comets is significantly shallower than the size frequency distribution of Jupiter Family comets. **The corresponding values of r_{min} for the two populations are** $1.55^{+0.22}_{-0.20}$ **and** $2.03^{+0.78}_{-0.68}$**, respectively.**

The test of statistical significance outlined in the previous paragraph results in a fraction of 36% of artificial data having a lower probability than the Jupiter Family data. For the isotropic comets this fraction is 34%. From the KS-test, we get a significance of 11.4% for the Jupiter Family data, and 3.3% for the isotropic comet data set. We can therefore conclude that our assumptions are statistically in agreement for the Jupiter Family data set. For the isotropic comet data set, the significance of the KS-test is low, and our assumption of a single underlying power law over the full range of nuclear sizes, with additional normal noise, therefore questionable.

[Figure 5]

17

4.3 Potential biases in the frequency distributions

The frequency distributions presented in this work are strongly affected by observational biases. The probability of discovery of a comet depends on its orbital parameters, determining the geometrical observability of the object (i.e. the heliocentric and geocentric distances and the solar elongation), and the absolute magnitude of the object. Comets of the Jupiter Family are typically observed at smaller heliocentric and geocentric distances than isotropic comets, since they orbit closer to the Sun. Therefore, the detection of smaller objects is more likely in this class of comets than for isotropic comets.

In general, hardly any comet in our data set was observed when being fainter than about 20^{m} – 21^{m}. Therefore, the observations of comets of both classes are limited by the same apparent magnitude. Because of these effects, the distribution of the absolute nuclear magnitudes of distant comets, such as isotropic comets, could be biased towards lower values, compared to Jupiter Family comets. The observation that much larger nuclei exist among the isotropic comets than among the Jupiter Family comets is not caused by an observational bias effect, since such large objects would be easy to discover within the relatively close Jupiter Family.

Within a class of comets, smaller objects, with larger absolute magnitudes, are expected to be underrepresented compared to larger objects. Therefore it is of interest to study the change in the slope of the size frequency distribution when progressively excluding data points corresponding to small radii. To do so, fits were performed to all data points larger than a certain limit r_{limit}, using r_{min} and α as free parameters. Table 4 presents the best fitting parameters for different values of r_{limit}, both for the Jupiter Family comets and the isotropic comets. The levels of significance of the fits according to the KS-test are also presented. It can be seen that the value of α is increases with increasing r_{limit}, and also the level of significance is increasing. However, if r_{limit} is getting large, the value of α is increasing dramatically, and the level of significance is decreasing again. This behavior shows that if the range in radii covered by the data points gets small, the differences in radius between different comets is more likely explained by the normally distributed noise component than by the power law distribution. If the range of radii over which data points are fitted is getting close to the standard deviation of the normally distributed noise, the value of α is increasing towards infinity, indicating that a constant radius for all comets included in the fitting, affected by noise, is the most likely model for the observed distribution. Fitting results for α are therefore not meaningful for large values of r_{limit}. As it is not clear at which value of r_{limit} the improvement in reliability of the fit due to reduced observational bias is canceled out by an unrealistically high weight of the noise, in the following discussion we use the values obtained with $r_{limit} = 0$, i.e. fitting to all available data points in each data set.

18

[Table 4]

4.4 Comparison of the frequency distributions of different comet classes

When comparing the absolute magnitude distribution of Jupiter Family comets and isotropic comets in Fig. 5, it can be noted that the distributions of absolute magnitudes of both populations extend to similar upper values. The largest absolute magnitude of isotropic comets in the data set is $18\overset{m}{.}5$, while the largest value for the Jupiter Family comets is $19\overset{m}{.}2$. This effect is probably caused by an observational bias, since almost no observations of objects with apparent magnitudes higher than 20^m were available. On the brighter end of the distributions, the situation is very different. The frequency of Jupiter Family comets drops strongly between the intervals of 12 to 13 magnitudes, and 11 to 12 magnitudes. The lowest absolute magnitude among the Jupiter Family comets in the data set is $11\overset{m}{.}3$. The absolute magnitudes of the isotropic comets extend to much lower values, down to $7\overset{m}{.}9$.

The derived exponents of the size frequency distributions **from fits to all data in each data set** are $2.01^{+0.21}_{-0.17}$ for the Jupiter Family, and $1.56^{+0.15}_{-0.12}$ for the isotropic comets. The slope of the size frequency distribution of isotropic comets in our data set is thus significantly shallower than the slope for the Jupiter Family comets. Furthermore, it can be seen that, as the magnitude frequency distribution of isotropic comets extends to lower values, the size frequency distribution extend to much larger values than the one for the Jupiter Family comets. While the largest Jupiter Family comet in our data set has a radius of 15.5 km, the isotropic comets reach radii up to 76.1 km.

4.5 Comparison with other frequency distributions

The size frequency distributions of Jupiter Family comets has been subject to detailed studies during the last decade. Exponents for the slope of the cumulative size frequency distributions have been published by different groups. These values were derived from different studies, such as HST observations with subtraction of the coma (Lamy et al. 2004), observations of distant comets (Lowry et al. 2003, Meech et al. 2004), and analysis of archived magnitude estimates (Tancredi et al. 2006). The exponents of the size frequency distributions were determined on different size intervals, and with different selection criteria (e.g. the perihelion distance of the comets). After converting the presented exponents of the cumulative size frequency distributions to the exponent of the differential distribution, and adopting the convention that the negative sign is not included, as in this work, the slope parameters α range from 2.45 ± 0.05 (Meech et al. 2004) to 3.7 ± 0.3 (Tancredi et al. 2006). Even for data from a single publication, a strong variation in the slope depending on the size interval used for the fit can be observed, e.g. between 2.66 for a fit to all nuclear sizes larger than 0.9 km to 3.50 when fitting only to nuclear sizes between 1.5 km and 5 km in

the data by Lamy et al. (2004). Furthermore, size frequency distributions were derived for populations of objects correlated with comets, such as dormant Jupiter Family comets (2.5 ± 0.3, Whitman et al. 2006), and asteroids on cometary orbits, i.e. having a Tisserand parameter with respect to Jupiter less than 3 (3.55 ± 0.04, Alvarez-Candal & Licandro 2006). The reasons for the large differences in the size frequency distributions by different working groups is not fully clear. Among the causes for the deviations might be the influence of the range of sizes over which the size frequency distribution is determined, as well as uncertainties in albedo, phase function, and the photometric uncertainty (Weissman et al. 2009). However, also selection effects and the presence of cometary activity could affect the derived slope parameters.

The differential slope parameter for Jupiter Family comets derived in this work, $\alpha = 2.01^{+0.21}_{-0.17}$, is smaller than any of the values presented by now. The large difference to other results could be caused by several effects:

First, the comets studied in this work could be physically different from the comets studied by other authors. In this work, comets are studied that show unusual activity in the sense that some show only insignificant activity compared to the brightness of the nucleus (e.g. Comet 162P/Siding Spring), or show only periods of activity being not symmetric with respect to the perihelion (e.g. Comet C/2001 OG$_{108}$ LONEOS). These objects could have a different size frequency distribution compared to "regular" comets.

Second, the comets in this work are affected by observational selection effects. Different to the work by Whitman et al. (2006), no correction was applied to remove the effect of biases in the discovery of comets arising from their orbital elements and absolute magnitudes. Furthermore, since comets with low activity are studied, biases in the discovery could be even stronger than for comets with regular activity. Such discovery biases would result in an overrepresentation of large cometary nuclei in our data set, and thus an higher value for the slope of the size frequency distribution, compared to the study by Whitman et al. (2006).

Third, the observations analyzed in this work could be affected by undiscovered activity, influencing the slope of the size frequency distribution derived from these observations. Such cometary activity would result in an underestimation of the nuclear magnitudes.

Apart from these potential sources of discrepancy, different exponents of the size frequency distributions could also arise from the different fitting methods applied in the mentioned publications, e.g. linear fits to a subset of the nuclear sizes in logarithmic space. Therefore, a re-evaluation of the nuclear size frequency distribution of the Jupiter Family comets with published radii, using the same fitting method as applied in this work, would be desirable for a comparison with the results of this work. This re-evaluation is presented in the following subsection.

For the isotropic comets, no slope parameter for the size frequency distribution was presented in the literature previously. The parameter derived in this work, $1.56^{+0.15}_{-0.12}$, indicates a shallower size frequency

20

distribution for these comets than for Jupiter Family comets. Meech et al. (2004) summarize the known radii of six isotropic comets, and they present upper limits for five additional isotropic comets they did not detect during dedicated observations. In order to test whether the non-detection of these five comets contradicts the results of this work, we compute the probability of randomly selecting five isotropic comets from a power law with $\alpha = 1.56$ and having comets smaller than the 2–σ upper limits presented by Meech et al. (2004). For this purpose we assume that the power law extends from infinity down to the radius of the smallest isotropic comet known to date, C/1983 J1 Sugano-Saigusa-Fujikawa with a radius of 0.37 km (Hanner et al. 1987). The resulting probability for obtaining by chance five comets with the specified upper limits of 10.5 km, 6.4 km, 4.0 km, 5.9 km, and 6.1 km, respectively, is 31.1%. Thus, the non-detection of these five comets is not conflicting with the result on the power law exponent α from this work.

4.6 Re-evaluation of the size frequency distribution of Jupiter Family comets

For comparing the results on the size frequency distribution of Jupiter Family comets with results from other works, it is desirable to use the same method in fitting a power law to the set of nuclear radii. The fitting method described in section 4.1 requires the knowledge of the uncertainty of each nuclear radius in the data set from which α is to be determined. As the largest published data sets do not provide sufficiently accurate errors, we cannot apply the fitting method of this work straight to data sets of different publications. Thus, a new data set of Jupiter Family comet radii from the literature has to be compiled. When doing so, we applied the strict definition of a Jupiter Family comet as having a Tisserand parameter between 2 and 3. Table 5 provides an overview over the radii of comets we took into consideration. When compiling the data set of radii from a literature search, except the requirement of an individual error estimate, several other criteria were applied. First, if nuclear size determinations from spacecraft flybys are available for one comet, these sizes were regarded as the best determination, and no other size determinations for these comets were taken into consideration. If several size determinations for a particular comet are available, different priorities were given to the different values. If a particular size determination includes an analysis of the light curve variation of a comet, and a variation of the light curve was detected, this value was given priority compared to size determinations from "snapshot" observations. If several size determinations from snapshot observations for a comet are available, or not variation in its lightcurve was detected, all available size determinations were averaged. This was done by computing the weighted mean of all individual radii available. By doing so, we can reduce the available sizes for one comet to a single one.

When combining radii for different comets and from different sources, problems could arise from different assumptions on the albedo and the phase function made for deriving the sizes. For the albedo, for most comets the standard value for the geometric albedo of 0.04 was used. For few comets, individual

21

albedo values were available and were used. Were size determinations with both, the standard albedo and an individual albedo were available, and the values differ, priority was given to the size derived with the individual albedo. The only comets for which this was the case are 45P/Honda-Mrkos-Pajdusakova and 103P/Hartley 2. Therefore, no significant effects upon the determination of α is expected as far as the albedo is concerned. For the phase function, a linear phase law was assumed throughout. However, the parameter of the assumed phase law ranges from 0.03 to 0.04 magnitudes per degree. For these differences, no correction was included. Finally we arrive at a set of 46 Jupiter Family comets, and thus a data set of the same size than the one produced in this work.

When applying the fitting method of section 4.1 to this literature data set, the very different accuracies of the radii prevent us from assuming a simple relationship between the standard deviation σ of the normal noise contribution, and the radius r of the nucleus. Therefore, one has to think in terms that every radius in this work was drawn from a different distribution having the same parameter α but different functions for $\sigma(r)$. If we assume that we know $\sigma(r)$ for each of these individual distributions, we can nevertheless compute the total probability of the data set, and thus maximize that probability to obtain the best fit value for α. As it is not clear how $\sigma(r)$ looks like for the different comets, we try two different simple assumptions. First, we assume $\sigma(r)$ to be constant, where σ is given in Table 5 for each comet. Second, we assume that the relative error, i.e. $\sigma(r)/r$, is constant, as we did for our own data set. It turns out that the resulting value of α is about the same for these two assumptions.

With the assumption of a constant σ, the literature data set of Jupiter Family comets is best fitted with $\alpha = 1.98^{+0.16}_{-0.14}$ **and** $r_{min} = 0.623^{+0.022}_{-0.025}$. For the assumption of a constant relative error, the result is $\alpha = 1.97^{+0.16}_{-0.14}$. Thus, when fitting the size frequency distribution of Jupiter Family comets with radii published in the literature with the same fitting method as used for the data set of this work, the resulting values of the parameter α are in good agreement. However, as the nuclear radii from the literature have to be thought as drawn from different size frequency distributions, a KS-test cannot be performed to verify the significance of the model applied.

Table 4 shows the fit results for α and r_{min} for different values of r_{limit}, computed assuming a constant σ.

[Table 5]

5   Discussion

Although the uncertainty on the results derived here from an inhomogeneous data base is considerable, we outline below some implications of our findings.

5.1 Implications for the size frequency distributions

The observation that much larger nuclei may exist among the isotropic comets than among the Jupiter Family comets can be explained by four different processes.

First, in general there are more isotropic comets known than Jupiter Family comets. It thus could be more likely to have larger nuclei among the known isotropic comets than among the known Jupiter Family comets, even if the size distribution is the same for both populations. However, after applying homogeneous selection criteria to all comet discoveries within a certain time interval, we ended up with slightly less isotropic comets than Jupiter Family comets in our data set. Yet, still we find significantly larger nuclei among the smaller set of isotropic comets. It is therefore unlikely that this result is caused by different numbers of comets of different dynamical classes in our data sets.

Second, it could be assumed that the albedo of distant isotropic comet nuclei is higher than for Jupiter Family comets. The higher albedo could make these comet nuclei appear larger than they are. However, a comparison of albedos of twelve Jupiter Family cometary nuclei with the albedos of seven isotropic comets show no significant difference (Lamy et al. 2004). This explanation appears therefore unlikely.

Third, the lack of large nuclei within the Jupiter Family can be due to a larger dynamical age of these comets. If these objects have encountered the inner Solar System more frequently than isotropic comets, and have been heated by solar irradiation more severe, splitting events might have occurred more often for these comets. Such splitting events are observed frequently among comets (Boehnhardt 2004), and it could lead to progressive reduction of the nuclear sizes.

Fourth, the observed differences between the sizes of the two comet classes could reflect differences in the sizes of objects in the source regions, i.e. there are larger nuclei in the Oort cloud, observed as isotropic comets, than in the Transneptunian region, observed as Jupiter Family comets. Such a difference would be reasonable if it is assumed that the collisonal processing of the Oort Cloud population is different than that of the Transneptunian population. To address this possibility further, more information on the size frequency distribution is needed, requiring further observation and removal of observational biases.

5.2 Implications for the structure of cometary nuclei

For some dynamically evolved comets in the data set, the existence of periodic cometary activity along the orbit is confirmed, e.g. for the Halley-type comet C/2001 OG_{108}. Also the very low cometary activity of the Jupiter Family comet 162P was confirmed. Such behavior can be well explained by the presence of small, located icy areas on the surface of the object, as for C/2001 OG_{108}, or general low content of volatile material. Generally, it is assumed that such small or isolated icy regions result from surface alteration during a larger number of passages through the inner Solar System. The sublimation of volatiles is assumed

23

to result in the formation of a crust depleted in volatiles, thus restricting the activity of an object.

For dynamically new comets, as present in the analyzed data set, such an explanation cannot be applied. These comets enter the inner Solar System for the first time, and no surface alteration due to solar irradiation is expected. Other mechanisms could also lead to sudden increase in cometary activity at some point of the orbit, such as phase transitions of ice, or depletion in hypervolatile material. However, as can be seen from Table 2, the discovery of activity of the objects in the data set is not correlated with heliocentric distance, as would be expected in such alternative explanations (e.g. depletion in hypervolatiles should result in an onset of activity at about 3 AU, where water starts to sublimate efficiently). Thus, a low content of isolated volatiles would provide the best explanation for unusual activity also for dynamically new comets. This would imply low volatile contents in some cometary nuclei not resulting from depletion of volatiles close to perihelion, but rather as a primordial characteristic.

Future comet observations could therefore be useful to confirm the nuclear magnitude estimates for some comets presented in this work. Such observations could also help to confirm the assumed inactivity of isotropic comets at some part of their orbit. If such inactivity can be confirmed for dynamically new isotropic comets, implications for the bulk composition of comets could be derived as far as the content of volatile material is concerned. Furthermore, data by future sky survey programs, such as PAN-STARRS (Jedicke 2008) or Gaia (Cellino et al. 2005), could then be used to further constrain the size frequency distributions of comets of all dynamical classes.

6 Summary

In this work we present estimates of the absolute nuclear magnitudes, nuclear radii, and the size frequency distributions of comets of different dynamical classes. Published survey observations of comets classified as point-like objects were used. For five comets in the analyzed data set of 84 comets, a comparison of the nuclear magnitudes or nuclear sizes with results of independent studies were possible, showing a satisfactory agreement in all cases. Significant differences in the frequency distributions of absolute nuclear magnitudes between Jupiter Family comets and isotropic comets were found. The absolute magnitudes of isotropic comets extend to much lower values than the corresponding distribution for Jupiter Family comets. The slope of the size frequency distribution of the isotropic comets were found to be shallower than the size frequency distribution of Jupiter Family comets.

However, the presented properties of comet classes could be influenced observational bias effects. Furthermore, from the limited available information on the comets analyzed in this work, disturbing influences by undetected cometary activity cannot be ruled out for all comets in the data set of this work. Nevertheless, the differences in size distributions found here form a basis for further, dedicated observations which will

help to address these findings with higher measurement accuracy.

References

Abell, P. A., Fernández, Y. R., Pravec, P., French, L. M., Farnham, T. L., Gaffey, M. J., Hardersen, P. S., Kušnirák, P., Šarounová, L., Sheppard, S. S., and Narayan, G. 2005, Physical characteristics of Comet Nucleus C/2001 OG$_{108}$ (LONEOS), Icarus, 179, 174–194

A'Hearn, M. F., Belton, M. J. S., Delamere, W. A., et al. 2005, Deep Impact: Excavating comet Tempel 1, Science, 310, 258–264

Alvarez-Candal, A., and Licandro, J. 2006, The size distribution of asteroids in cometary orbits and related populations, A&A, 458, 1007–1011

Bagatin, A. C. 2006, Collisional evolution of asteroids and Trans-Neptunian objects, Proceedings of the IAU Symposium 229, Asteroids, Comets, Meteors, 229, 335–350

Boehnhardt, H., Rainer, N., Birkle, K., and Schwehm, G. 1999, The nuclei of comets 26P/Grigg-Skjellerup and 73P/Schwassmann-Wachmann 3, A&A, 341, 912–917

Boehnhardt, H. 2004, Split Comets, in: Comets II, 301–316

Bowell, E., Hapke, B., Domingue, D., et al. 1989, Asteroids II, ed. Binzel et al. (Univ. of Arizona Press), 524-556

Brownlee, D. E., Horz, F., Newburn, R. L., et al. 2004, Surface of young Jupiter Family comet 81P/Wild 2: View from the Stardust spacecraft, Science, 304, 1764–1769

Cellino, A., Tanga, P., Mignard, F., dell'Oro, A., Hestroffer, D., Muinonen, K., Petit, J. M., Thuillot, W., and Gaia Solar System Working Group Team 2005, Gaia: an unprecedented tool for Solar System Science,

Bulletin of the American Astronomical Society, 37, 1564

Clark, B. E., Veverka, J., Helfenstein, P., Thomas, P. C., Bell, J. F., Harch, A., Robinson, M., S., Murchie, S. L., McFadden, L. A., and Chapman, C. R. 1999, NEAR Photometry of Asteroid 253 Mathilde, Icarus, 140, 53–65

Clark, B. E., Helfenstein, P., Bell, J. F., Peterson, C., Veverka, J., Izenberg, N. I., Domingue, D., Wellnitz, D., and McFadden, L. A. 2002, NEAR Infrared Spectrometer Photometry of Asteroid 433 Eros, Icarus, 155, 189–204

Delahodde, C. E., Meech, K. J., Hainaut, O. R., and Dotto, E. 2001, Detailed phase function of comet 28P/Neujmin 1, A&A, 376, 672–685

Despois, D., Biver, N., Bockelée-Morvan, D., and Crovisier, J. 2005, Observations of molecules in comets, Proceedings of the IAU symposium 231, Astrochemistry: Recent Successes and Current Challenges, 231, 469–478

Fernández, Y. R., Campins, H., Kassis, M., Hergenrother, C. W., Binzel, R. P., Licandro, J., Hora, J. L., and Adams, J. D. 2006, Comet 162P/Siding Spring: A Surprisingly Large Nucleus, AJ, 132, 1354–1360

Grimmett, G., and Welsh, D., 1986, Probability: An Introduction, Oxford University Press

Fink, U. 1994, The trend of production rates with heliocentric distance for comet P/Halley, ApJ, 423, 461–473

Groussin, O., Lamy, P., Jorda, L., and Toth, I. 2004, The nuclei of comets 126P/IRAS and 103P/Hartley 2, A&A, 419, 375–383

Groussin, O., Lamy, P., Toth, I., Kelley, M., Fernandez, Y., A'Hearn, M., Campins, H., Licandro, J., Lisse, C., Lowry, S., Meech, K., and Snodgrass, C. 2009, The size and thermal properties of the nucleus of comet 22P/Kopff, Icarus, 199, 568–570

Hanner, M. S., Newburn, R. L., Spinrad, H., and Veeder, G. J. 1987, Comet Sugano-Saigusa-Fujikawa (1983V) – a small, puzzling comet, AJ, 94, 1081–1087

Helin, E. F., Pravdo, S. H., Lawrence, K. J., Hicks, M. D., and NEAT Team 2000, The Near-Earth Asteroid Tracking (NEAT) Program, Bulletin of the American Astronomical Society, 32, 750

Hicks, M. D., and Bauer, J. M. 2007, P/2006 HR30 (Siding Spring): A Low-Activity Comet in Near-Earth Space, ApJ, 662, L47–L50

Hicks, M. D., Bambery, R. J., Lawrence, K. J., and Kollipara, P. 2007, Near-nucleus photometry of comets using archived NEAT data, Icarus, 188, 457–467

Jedicke, R. 2008, Pan-STARRS: First Solar System Results, LPI Contributions, 1405, 8301

Jewitt, D. 2002, From Kuiper Belt object to cometary nucleus, ESASP 500: ACM 2002, 11–19

Jewitt, D., Sheppard, S., and Fernández, Y. 2003, 143P/Kowal-Mrkos and the shapes of cometary nuclei, AJ, 125, 3366–3377

Jewitt, D. 2005, A first Look at the Damocloids, AJ, 129, 530–538

Jewitt, D., Lacerda, P., and Peixinho, N. 2007, Comet 133P/Elst-Pizarro, IAU Circular 8847

Jurić, M., et al. 2002, Comparison of positions and magnitudes of asteroids observed in the Sloan Digital Sky Survey with those predicted for known asteroids, AJ, 124, 1776–1787

Kelley, M. S., Reach, W. T., and Lien, D. J. 2008, The dust trail of comet 67P/Churyumov-Gerasimenko, Icarus, 193, 572–587

Kirk, R. L., Duxbury, T. C., Hörz, F., Brownlee, D. E., Newburn, R. L., Tsou, P., and The Stardust Team, 2005, Topography of the 81/P Wild 2 Nucleus Derived from Stardust Stereoimages, Lunar and Planetary Inst. Technical Report, 36, 2244

Koehn, B. W., and Bowell, E. L. G. 2000, Bulletin of the American Astronomical Society, 32, 1018

Koen, C., and Kondlo, L. 2009, Fitting power law distributions to data with measurement errors, MN-

RAS, 397, 495–505

Lamy, P. L., Toth, I., Jorda, L., Weaver, H. A., and A'Hearn M. F. 1998a, The nucleus and inner coma of comet 46P/Wirtanen, A&A, 335, L25–L29

Lamy, P. L., Toth, I., and Weaver, H. A. 1998b, Hubble Space Telescope observations of the nucleus and inner coma of comet 19P/1904 Y2 (Borrelly), A&A, 337, 945–954

Lamy, P. L., Toth, I., A'Hearn, M. F., and Weaver, H. A. 1999, Hubble Space Telescope observations of the nucleus of comet 45P/Honda-Mrkos-Pajdusakova and its inner coma, Icarus, 140, 424–438

Lamy, P. L., Toth, I., Jorda, L., Groussin, O., A'Hearn, M. F., and Weaver, H. A. 2002, The nucleus of comet 22P/Kopff and its inner coma, Icarus, 156, 442–455

Lamy, P. L., Toth, I., Fernandez, Y. R., and Weaver, H. A. 2004, The sizes, shapes, albedos, and colors of cometary nuclei, in: Comets II, 223–264

Lamy, P. L., Toth, I., Groussin, O., Jorda, L., Kelley, M. S., and Stansberry, J. A. 2008, Spitzer Space Telescope observations of the nucleus of comet 67P/Churyumov-Gerasimenko, A&A, 489, 777–785

Lamy, P. L., Toth, I., Weaver, H. A., A'Hearn, M. F., and Jorda, L. 2009, Properties of nuclei and comae of 13 ecliptic comets from Hubble Space Telescope snapshop observations, A&A, 508, 1045–1056

Levison, H. F. 1996, Comet Taxonomy, in: Completing the Inventory of the Solar System, Astronomical Society of the Pacific Conference Series, 107, 173–191

Lisse, C. M., Fernandez, Y. R., Reach, W. T., Bauer, J. M., A'Hearn, M. F., Farnham, T. L., Groussin, O., Belton, M. J., Meech, K. J., and Snodgrass, C. D. 2009, Spitzer Space Telescope observations of the nucleus of comet 103P/Hartley 2, PASP, 121, 968–975

Lowry, S. C., Fitzsimmons, A., Cartwright, I. M., and Williams, I. P. 1999, CCD photometry of distant comets, A&A, 349, 649–659

Lowry, S. C., and Fitzsimmons, A. 2001, CCD photometry of distant comets II, A&A, 365, 204–213

Lowry, S. C., Fitzsimmons, A., and Collander-Brown, S. 2003, CCD photometry of distant comets. III. Ensemble properties of Jupiter-family comets, A&A, 397, 329–343

Lyons, L., 1986, Statistics for nuclear and particle physicists, Cambridge University Press

Mallama, A., Wang, D., and Howard, R. A. 2002, Photometry of Mercury from SOHO/LASCO and Earth. The Phase Function from 2 to 170 deg., Icarus, 155, 253–264

Meech, K. J., Hainaut, O. R., and Marsden, B. G. 2004, Comet nucleus size distributions from HST and Keck telescopes, Icarus, 170, 463–491

Newman, M. E. J. 2005, Power laws, Pareto distributions and the Zipf's law, Contemporary Physics, 46, 323–351

Oberst, J., Giese, B., Howington-Kraus, E., Kirk, R., Soderblom, L., Buratti, B., Hicks, M., Nelson, R. and Britt, D. 2004, The nucleus of Comet Borrelly: a study of morphology and surface brightness, Icarus, 167, 70–79

Piironen, J., Lagerkvist, C.-I., Erikson, A., Oja, T., Magnusson, P., Festin, L., Nathues, A., Gaul, M., and Velichko, F. 1998, Physical studies of asteroids. XXXII. Rotation periods and UBVRI-colours for selected asteroids, A&AS, 128, 525–540

Press, W. H., Teukolsky, S. A., Vetterling, W. T., and Flannery, B. P., 2007, Numerical Recipes, Third edition, Cambridge University Press

Russell, H. N. 1916, On the Albedo of the Planets and their Satellites, ApJ, 43, 173–196

Snodgrass, C., Fitzsimmons, A., and Lowry, S. C. 2005, The nuclei of comets 7P/Pons-Winnecke, 14P/Wolf and 92P/Sanguin, A&A, 444, 287–295

Snodgrass, C., Lowry, S. C., and Fitzsimmons, A. 2006, Photometry of cometary nuclei: rotation rates, colours and a comparison with Kuiper Belt Objects, MNRAS, 373, 1590–1602

Stokes, G. H., Evans, J. B., Viggh, H. E. M., Shelly, F. C., and Pearce, E. C. 2000, Lincoln Near-Earth Asteroid Program (LINEAR), Icarus, 148, 21–28

Szabó, G. M., Kiss, L. L., and Sárneczky, K. 2008, Cometary Activity at 25.7 AU: Hale-Bopp 11 Years after Perihelion, ApJ, 677, L121–L124

Tancredi, G., Fernández, J. A., Rickman, H., and Licandro, J. 2000, A catalog of observed nuclear magnitudes of Jupiter family comets, A&ASS, 146, 73–90

Tancredi, G., Fernández, J. A., Rickman, H., and Licandro, J. 2006, Nuclear magnitudes and the size distribution of Jupiter Family comets, Icarus, 182, 527–549

Thomas, P. C., Veverka, J., Simonelli, D., Helfenstein, P., Carcich, B., Belton, M. J. S., Davies, M. E., and Chapman, C. 1994, The shape of Gaspra, Icarus, 107, 23–36

Thomas, P. C., Belton, M. J. S., Carcich, B., Chapman, C. R., Davies, M. E., Sullivan, R., and Veverka, J. 1996, The shape of Ida, Icarus, 120, 20–32

Weissman, P. R., Snodgrass, C., Fitzsimmons, A., and Lowry, S. C. 2009, The Size Distribution of Jupiter-Family Comet Nuclei, DPS meeting 41, 23.13

Whitman, K., Morbidelli, A., and Jedicke, R. 2006, The size frequency distribution of dormant Jupiter Family comets, Icarus, 183, 101–114

Appendix A

Section 4.1 presented an approach for determining the exponent of a power law distribution from sparse and noisy data. In order to show the need for such an improved approach in case of significant noise, and to verify its suitability, we performed tests using random generated artificial data. In a first step we were producing 5000 sets of 30 random numbers drawn from a power law with the known parameter $\alpha = 2.5$ on the interval $[3.0, \infty]$. For each of these sets, we first determined the parameter α by using the approach for noiseless data presented by Newman (2005). Then, a normally-distributed noise component was added to the artificial data. Two different cases were regarded. First, a constant value for the standard deviation of the normal component, $\sigma = 1.5$, was used. Second, a value of σ depending linearly on the noiseless value r was used, having the form $\sigma(r) = 0.3\ r$. Fig. 6 shows the distribution of α obtained by fitting the different sets of 30 data points with the method by Newman (2005). The solid line in panel (a) shows the distribution obtained for the noiseless test data, while the shaded histogram shows the resulting distribution for the noisy data, with constant σ. While in the noiseless case the method by Newman (2005) results in a distribution centered on the correct value of α, as expected, in the noisy case a clear bias with respect to the true value can be observed. Panel (b) shows the same situation but with a value of σ depending on r. Again, the distribution of α obtained from fitting the 5000 sets of artificial data shows a bias with respect to the true value if noise is added. This illustrates the need for taking the effect of noise into account when determining the parameter α from noisy data.

To show the results obtained with the method described in section 4.1 on noisy data, we produced artificial data sets with the same properties already described. Then, these data sets were fitted with the method of section 4.1, using α and the lower limit of the interval from which the noiseless data points were drawn as free parameters. Fig. 7 shows the distributions of the the two parameters obtained from 5000 data sets and for the case of constant σ. The upper panel presents the distribution of the parameter α, the lower for the lower limit of the interval. It can be seen that both distributions are centered on the correct values. Fig. 8 shows the same distributions for 1000 artificial data sets and the case of varying σ. Again, the distributions for the two fitting parameters are centered on the true values. This illustrates that with the fitting method described in this work, the true parameters of the power law underlying a set of sparse and noisy data can be recovered.

[Figure 6]

[Figure 7]

[Figure 8]

Figure captions

Figure 1. Reduced magnitudes of comet C/2001 OG$_{108}$ versus time. The dotted line indicates the time of perihelion passage. A period of activity can be identified by an increase in the reduced magnitudes from about 60 days before perihelion to about 20 days after perihelion. In the lower part of the Figure, the variation of phase angle with time is shown.

Figure 2. Difference between the theoretically expected and observed magnitudes versus phase angle for the asteroids Eros and Mathilde. The different symbols refer to different observers. The dashed lines give the mean value from all observations, and the dotted lines the estimated uncertainty of $0^m.58$.

Figure 3. Cumulative number of comets with observed activity as a function of time between the discovery of the object and the discovery of its activity. 473 comet discoveries from 1998 to 2008 are included in this plot, not taking into account Soho discoveries. Pre-discovery observations are not considered in this plot.

Figure 4. Variation of brightness with heliocentric distance for all comets in the data set. All available observations of the objects are presented, also when the object was obviously active. The heliocentric distance is normalized to r_h at the time of discovery of activity, and ΔH denotes the difference between an individual absolute magnitude and the absolute magnitude determined by averaging all data points of one comet. Data points for three comets are highlighted by color: red: 162P/Siding Spring, green: P/2002 T6, blue: C/2002 T7.

Figure 5. Histogram of the absolute magnitudes of the comets in the analyzed data set. The histograms for the Jupiter Family comets (46 comets) and the isotropic comets (37 comets) are shown separately. The dotted curve shows absolute magnitudes for all 84 comets in the data set.

Figure 6. Distributions of the fitting parameter α for 5000 sets of 30 random data points, determined with the method by Newman (2005). The true value of α used when generating the data is indicated by the dotted lines. Panel (a). Solid line: distribution of α for noiseless test data. Shaded histogram: distribution for noisy data, with $\sigma = 0.15$. Panel (b). Solid line: distribution for noiseless data. Shaded histogram: distribution for noisy data, with $\sigma(r) = 0.3\ r$.

Figure 7. Distribution of the fitting parameters α (upper panel) and the lower limit (lower panel) for

5000 artificial data sets with 30 random points each. Noise with $\sigma = 0.15$ was added to the power law data. The parameters were determined with the method described in this work. The true parameter values used for the generation of the test data are indicated by dashed lines.

Figure 8. Same as Figure 7, but for 1000 sets of artificial data and $\sigma(r) = 0.3\ r$.
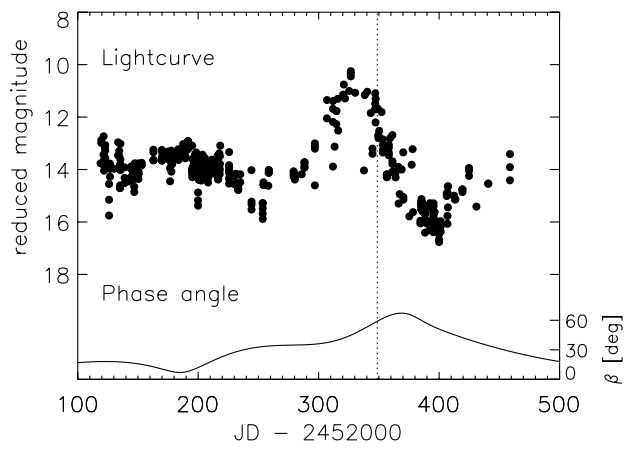
Figure 1: Weiler et al. Cometary nuclear magnitudes from sky survey observations
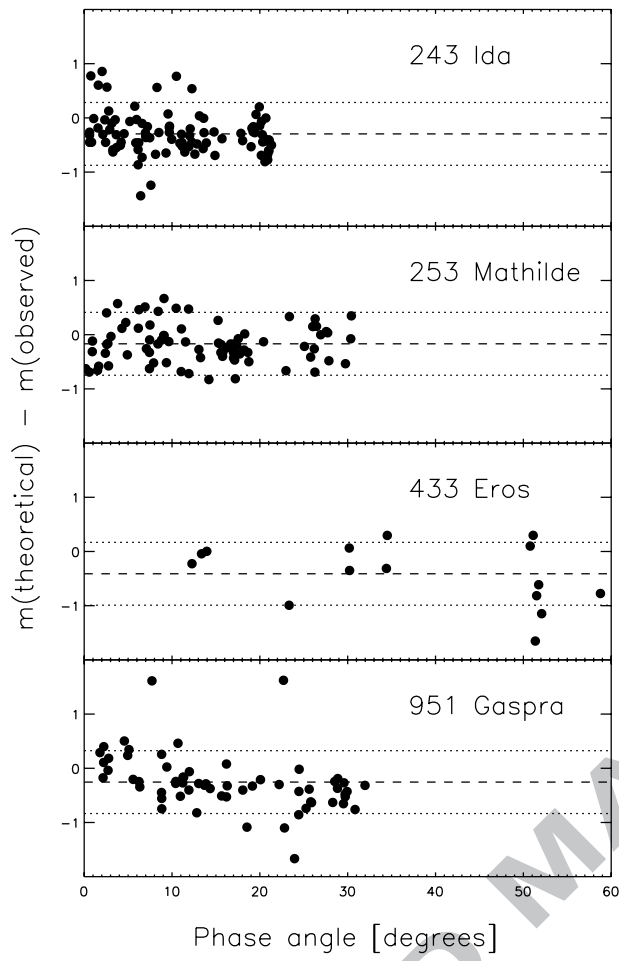
Figure 2: Weiler et al. Cometary nuclear magnitudes from sky survey observations
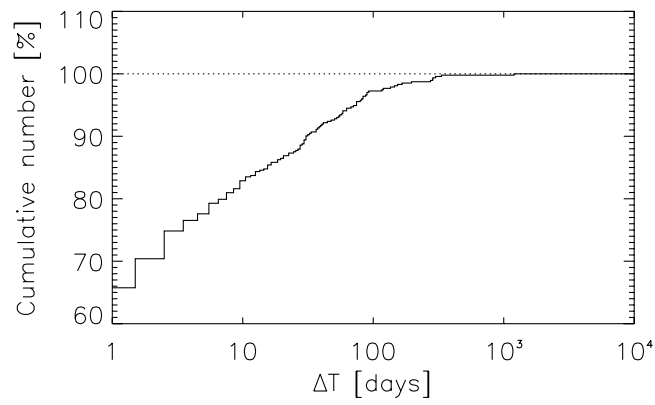
Figure 3: Weiler et al. Cometary nuclear magnitudes from sky survey observations.
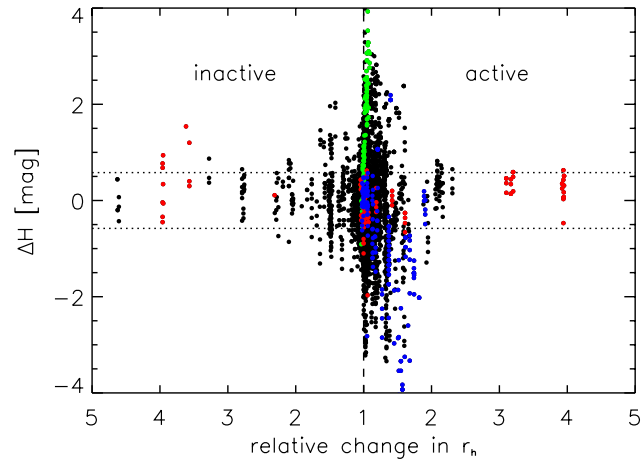
Figure 4: Weiler et al. Cometary nuclear magnitudes from sky survey observations.
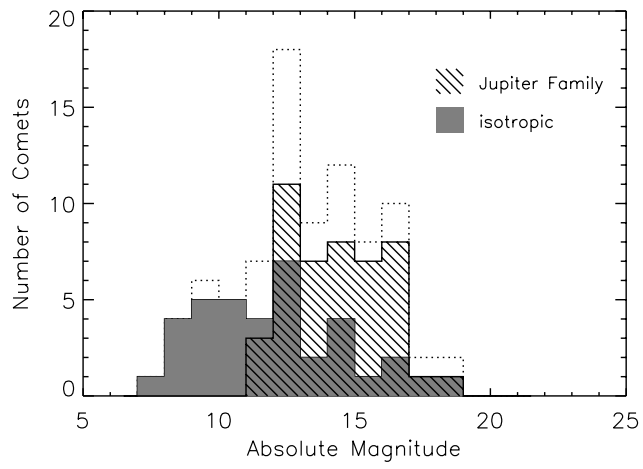
Figure 5: Weiler et al. Cometary nuclear magnitudes from sky survey observations.
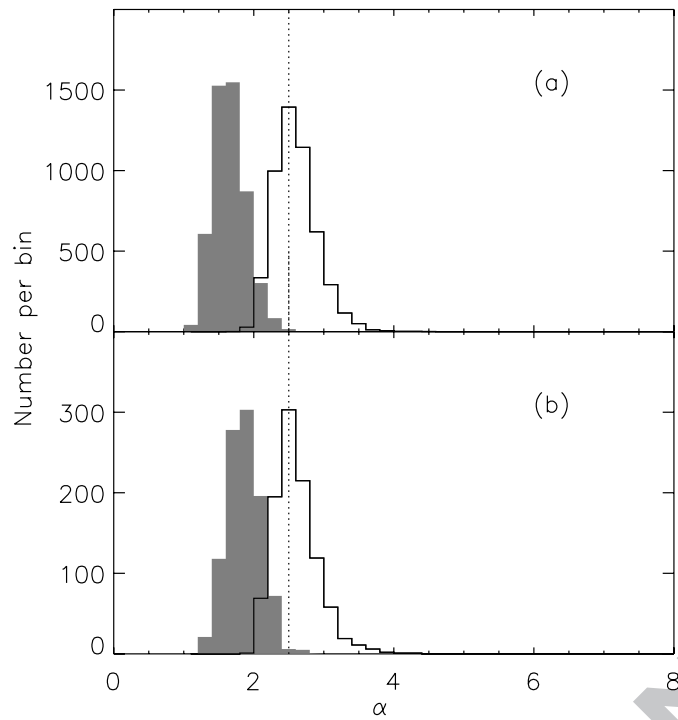
Figure 6: Weiler et al. Cometary nuclear magnitudes from sky survey observations.
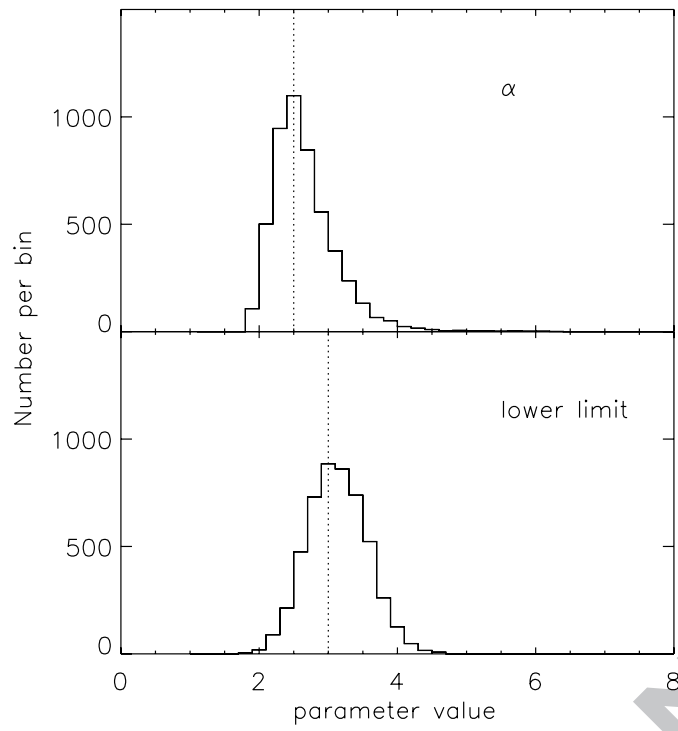
Figure 7: Weiler et al. Cometary nuclear magnitudes from sky survey observations.
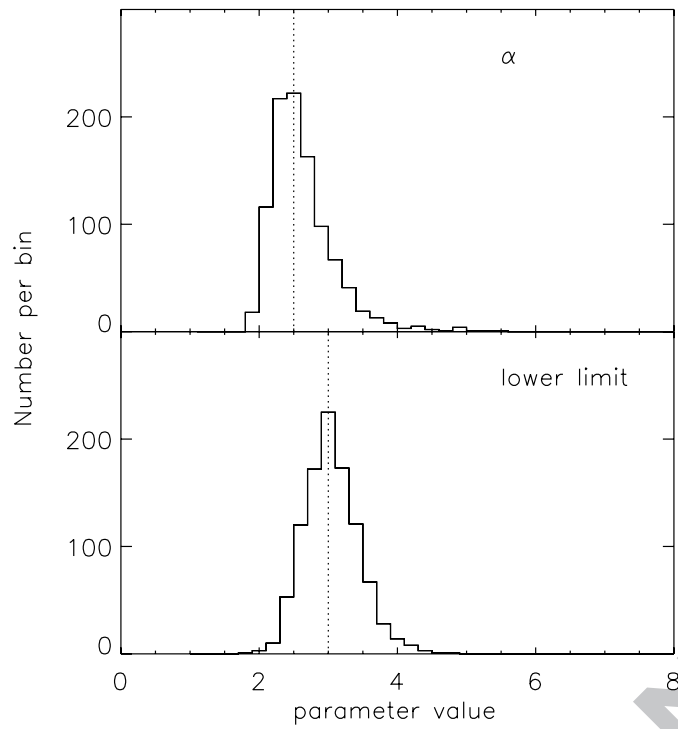
Figure 8: Weiler et al. Cometary nuclear magnitudes from sky survey observations.

Table 1: Biases in the magnitude estimates of asteroids for different observers. The observers are identified by their three-digit observatory code. The biases (Δm in magnitudes) with respect to observer 854 are presented. n gives the number of nearly simultaneous observations used for the determination of the bias.

difference for observers			Δm			n
926	–	854	−0.14	±	0.42	14
649	–	854	−0.18	±	0.31	14
673	–	854	−0.13	±	0.58	22
704	–	854	0.26	±	0.34	12
644	–	854	0.09	±	0.38	10
A50	–	854	−0.17	±	0.54	8
699	–	854	−0.32	±	0.25	12
I05	–	854	−0.09	±	0.82	6
703	–	854	−0.02	±	0.59	7
711	–	854	−0.23	±	0.83	10
291	–	854	0.35	±	0.35	22
691	–	854	0.31	±	0.29	11
608	–	854	1.19	±	0.41	10

42

Table 2: Basic parameters of the comets in the data set: comet designation, the date of discovery, the date of discovery of its activity, the perihelion distance q, inclination i, and eccentricity e, the heliocentric distance r_h^{act} at which activity was observed first, the dynamical type (DN - dynamically new, DO - dynamically old, JF - Jupiter Family, HT - Halley-type, CT - Chiron-type) and the IAUC number of reference.

Comet	Discovery			Discovery of Act.			q [AU]	i [°]	e	r_h^{act} [AU]	Type	IAUC
C/2008 E1	2008	3	2.1	2008	3	3.8	4.83	35.04	0.55	4.92	JF	8923
C/2007 O1	2007	7	17.2	2007	7	17.9	2.88	24.38	1.00	2.91	DN	8858
C/2007 D3	2007	2	20.1	2007	2	21.0	5.21	45.92	0.99	5.26	DO	8810
C/2007 D2	2007	2	17.5	2007	2	19.0	1.25	178.62	0.98	1.78	DO	8809
P/2007 C2	2007	2	9.1	2007	2	10.6	3.78	8.67	0.46	3.97	JF	8806
C/2007 VO$_{53}$	2007	11	1.3	2008	1	12.0	4.84	87.02	1.00	7.86	DN	8911
P/2007 VQ$_{11}$	2007	11	3.4	2008	2	1.2	2.69	12.32	0.50	2.69	JF	8914
C/2008 FK$_{75}$	2008	3	31.4	2008	7	3.2	4.52	61.15	1.00	7.71	DN	8958
P/2008 JK	2008	5	2.3	2008	9	17.4	1.19	15.10	0.67	1.20	JF	8978
P/2008 QP$_{20}$	2008	8	25.4	2008	9	24.3	1.72	7.75	0.51	1.76	JF	8979
C/2006 WD$_4$	2006	11	20.3	2007	4	30.8	0.59	152.70	1.00	0.59	DO	8835
P/2006 XG$_{16}$	2006	12	10.4	2007	1	27.2	2.10	9.08	0.42	2.10	JF	8802
C/2006 XA$_1$	2006	12	9.2	2007	1	9.1	1.80	30.63	0.99	2.96	DO	8790
C/2006 M1	2006	6	18.3	2006	6	22.0	3.56	54.88	0.98	4.13	DO	8724
P/2005 YQ$_{127}$	2005	12	28.3	2006	1	6.9	1.92	16.72	0.50	2.00	JF	8658
C/2005 G1	2005	4	1.4	2005	4	4.4	4.96	108.41	1.00	5.56	DN	8504
C/2006 VZ$_{13}$	2006	11	13.1	2006	12	1.1	1.02	134.79	1.00	3.65	DN	8781
C/2005 YW	2005	12	21.3	2006	10	11.2	1.99	40.54	0.99	2.11	DO	8760
C/2006 OF$_2$	2006	7	17.7	2006	9	20.1	2.43	30.17	1.00	7.24	DN	8756
P/2006 HR$_{30}$	2006	4	20.8	2006	7	29.3	1.23	31.88	0.84	2.37	HT	8735
C/2006 HW$_{51}$	2006	4	23.5	2006	6	4.3	2.27	45.81	1.00	2.62	DN	8718
P/2005 SB$_{216}$	2005	9	30.4	2005	12	7.0	3.82	24.10	0.46	4.56	JF	8668
P/2005 XA$_{54}$	2005	12	4.4	2006	1	6.4	1.78	16.90	0.71	1.89	JF	8656
C/2004 YJ$_{35}$	2004	12	31.1	2005	11	30.3	1.78	52.48	1.00	3.67	DN	8637
P/2005 RV$_{25}$	2005	9	11.3	2005	10	22.2	3.61	9.88	0.17	3.85	JF	8620
P/2004 FY$_{140}$	2004	3	27.3	2004	5	19.0	4.11	2.13	0.17	4.45	JF	8597
P/2005 JD$_{108}$	2005	5	12.4	2005	6	28.4	4.03	3.28	0.37	4.04	JF	8554
C/2005 EL$_{173}$	2005	3	8.2	2005	5	10.0	3.89	130.68	1.00	6.70	DN	8526
C/2004 X2	2004	12	8.5	2004	12	9.6	3.79	72.12	1.00	3.91	DO	8450
P/2004 VR$_8$	2004	11	3.3	2004	11	19.3	2.38	20.12	0.51	3.21	JF	8451
P/2004 WR$_9$	2004	11	22.3	2004	12	7.0	1.92	5.05	0.68	1.95	JF	8448
C/2004 RG$_{113}$	2004	9	6.4	2004	11	20.4	1.94	21.62	1.00	2.31	DO	8444
C/2004 K3	2004	5	29.3	2004	6	11.0	1.10	111.93	0.98	1.15	DO	8350
C/2004 HV$_{60}$	2004	4	25.3	2004	5	8.3	3.04	91.93	0.90	3.34	HT	8337
P/2004 EW$_{38}$	2004	3	14.5	2004	4	14.3	1.79	6.52	0.50	2.20	JF	8322
C/2004 DZ$_{61}$	2004	2	18.5	2004	3	16.0	2.01	66.81	0.96	2.18	DO	8321
C/2004 D1	2004	2	17.1	2004	2	20.8	4.97	45.54	1.00	7.30	DN	8294
P/2004 CB	2004	2	3.2	2004	3	30.8	0.91	19.15	0.69	0.91	JF	8314
P/2004 DO$_{29}$	2004	2	17.2	2004	3	16.3	4.09	14.53	0.45	4.26	JF	8305
P/2003 WC$_7$	2003	11	18.1	2004	2	1.2	1.65	21.22	0.68	1.66	JF	8280
P/2003 SQ$_{215}$	2003	9	24.2	2004	1	19.0	2.30	5.55	0.58	2.37	JF	8274
C/2003 WT$_{42}$	2003	11	19.3	2003	12	29.1	5.19	31.41	1.00	7.95	DN	8270
P/2003 UY$_{275}$	2003	10	29.3	2003	11	30.2	1.83	16.33	0.51	2.26	JF	8247
P/2003 QX$_{29}$	2003	8	23.3	2003	8	31.1	4.24	11.40	0.47	4.58	JF	8192
C/2002 X1	2002	12	5.4	2002	12	7.7	2.49	164.09	1.00	3.38	DO	8028
P/2002 LZ$_{11}$	2002	6	5.3	2003	10	29.0	2.37	11.52	0.35	2.77	JF	8240
C/2002 V2	2002	11	5.3	2002	11	7.1	6.81	166.78	1.00	6.92	DO	8013
C/2002 VQ$_{94}$	2002	11	11.2	2003	8	28.5	6.80	70.52	0.97	8.84	DO	8194
P/2003 HT$_{15}$	2003	4	26.3	2003	6	24.3	2.67	27.67	0.42	2.71	JF	8156
C/2002 T7	2002	10	14.4	2002	10	28.0	0.61	160.58	1.00	6.75	DN	8003
P/2002 T6	2002	10	4.5	2002	10	27.9	3.39	11.01	0.56	3.77	JF	8002
P/2002 T5	2002	10	5.4	2002	10	18.4	3.93	30.90	0.44	4.19	JF	7998
C/2002 L9	2002	6	13.4	2002	7	2.0	7.03	68.44	1.00	8.15	DO	7931

43

Table 2: Continued.

Comet	Discovery			Discovery of Act.			q [AU]	i [°]	e	r_h^{act} [AU]	Type	IAUC
P/2002 JN$_{16}$	2002	5	9.3	2002	5	17.2	1.79	11.41	0.49	1.90	JF	7907
C/2002 J5	2002	5	15.4	2002	5	16.0	5.73	117.23	1.00	6.70	DN	7904
P/2002 EJ$_{57}$	2002	3	13.2	2002	5	1.8	2.64	4.97	0.59	2.85	JF	7890
P/2002 AR$_2$	2002	1	6.1	2002	4	6.1	2.06	21.11	0.62	2.20	JF	7869
C/2002 A2	2002	1	8.3	2002	1	11.4	4.71	14.04	0.72	4.71	JF	7788
P/2002 CW$_{134}$	2002	2	7.5	2002	3	19.0	1.84	15.23	0.49	1.85	JF	7858
P/2001 YX$_{127}$	2001	12	17.3	2002	2	14.2	3.43	7.91	0.18	3.73	JF	7828
C/2002 B3	2002	1	26.1	2002	2	11.1	6.06	73.69	1.01	6.06	DN	7826
C/2002 B2	2002	1	23.4	2002	2	3.0	3.84	152.87	1.00	3.88	DO	7821
C/2001 OG$_{108}$	2001	7	28.4	2002	1	11.4	0.99	80.25	0.93	1.41	HT	7814
P/2001 TU$_{80}$	2001	10	13.4	2001	11	16.5	1.93	6.59	0.47	1.94	JF	7753
C/2001 RX$_{14}$	2001	9	10.3	2001	10	18.7	2.06	30.57	1.00	5.24	DN	7739
C/2001 G1	2001	4	1.2	2001	4	1.9	8.24	45.36	1.00	8.31	DN	7606
C/2001 A2	2001	1	15.0	2001	1	16.0	0.78	36.49	1.00	2.28	DO	7564
C/2000 SV$_{74}$	2000	9	24.3	2000	10	19.8	3.54	75.24	1.00	5.98	DN	7510
C/2000 OF$_8$	2000	7	24.3	2000	8	29.0	2.17	152.43	1.00	4.26	DN	7484
P/1999 XN$_{120}$	1999	12	5.2	2000	2	27.0	3.29	5.03	0.21	3.30	JF	7370
P/1998 VS$_{24}$	1998	11	10.3	1998	12	18.9	3.41	5.03	0.24	3.41	JF	7071
P/1998 QP$_{54}$	1998	8	27.4	1998	9	13.2	1.88	17.74	0.55	1.89	JF	7012
183P	1999	2	19.0	1999	5	14.0	3.90	18.73	0.14	3.97	JF	7167
182P	2001	11	17.3	2002	2	13.5	0.98	16.92	0.67	1.00	JF	7827
172P	2002	1	21.5	2002	5	5.0	2.24	11.52	0.36	2.28	JF	7896
169P	2002	3	15.3	2005	7	28.3	0.61	11.32	0.77	1.09	JF	8578
167P	2004	8	10.9	2005	6	7.4	11.78	19.12	0.27	12.41	CT	8545
162P	2004	10	10.6	2004	11	12.0	1.23	27.84	0.60	1.23	JF	8436
160P	2004	7	15.3	2004	9	6.6	2.08	17.26	0.48	2.10	JF	8408
159P	2003	10	16.4	2003	11	30.2	3.65	23.42	0.38	3.69	JF	8248
158P	2001	9	12.3	2003	11	26.4	4.59	7.90	0.03	4.64	JF	8244
150P	2000	11	25.4	2001	2	13.3	1.77	18.50	0.55	1.80	JF	7584
148P	2000	9	24.3	2000	11	24.3	1.70	3.68	0.54	2.24	JF	7524
139P	1998	11	18.3	1998	12	7.1	3.40	2.33	0.25	3.40	JF	7064

Table 3: Summary of the nuclear magnitudes and nuclear radii of the comets in the data set. The Table lists the comet designation, the absolute *R*-magnitude, the derived nuclear radius, the number of individual magnitude estimates, *n*, and the observers from which magnitude estimates were available. The uncertainty in absolute magnitude is estimated to be $0^m.58$, and the corresponding uncertainty in the nuclear radius is 27%.

Comet	type	H(1,1,0)	R_N [km]	*n*	Observers
C/2008 E1	JF	11.32	15.5	15	854 703
C/2007 O1	DN	12.80	8.1	21	704 703
C/2007 D3	DO	11.48	14.3	9	704
C/2007 D2	DO	17.48	0.9	6	691
P/2007 C2	JF	12.87	7.9	23	704 703 691
C/2007 VO$_{53}$	DN	11.11	16.9	6	691
P/2007 VQ$_{11}$	JF	14.17	4.3	24	699 703
C/2008 FK$_{75}$	DN	9.94	29.1	13	703
P/2008 JK	JF	17.37	1.0	8	703
P/2008 QP$_{20}$	JF	16.99	1.2	10	704 703
C/2006 WD$_4$	DO	16.61	1.4	7	854 711 291
P/2006 XG$_{16}$	JF	16.07	1.7	25	704 644 691
C/2006 XA$_1$	DO	12.60	8.6	24	704
C/2006 M1	DO	11.21	16.3	12	704 703
P/2005 YQ$_{127}$	JF	15.42	2.4	48	704 691
C/2005 G1	DN	10.87	18.9	12	673 704
C/2006 VZ$_{13}$	DN	13.33	6.1	17	854 673 704
C/2005 YW	DO	13.05	6.9	14	854 673 704
C/2006 OF$_2$	DN	9.26	40.7	15	854 644
P/2006 HR$_{30}$	HT	12.19	10.3	27	704 644 703
C/2006 HW$_{51}$	DN	12.80	7.7	3	854
P/2005 SB$_{216}$	JF	12.68	8.2	21	704 699 691
P/2005 XA$_{54}$	JF	14.84	3.0	21	704 699 703
C/2004 YJ$_{35}$	DN	14.96	3.0	91	649 704 699 703 711
P/2005 RV$_{25}$	JF	12.80	8.0	20	704 699 703
P/2004 FY$_{140}$	JF	12.29	10.0	39	704 699 703 691 608
P/2005 JD$_{108}$	JF	11.86	12.5	9	644 699 703
C/2005 EL$_{173}$	DN	10.98	17.9	12	704 699 691
C/2004 X2	DO	12.15	10.5	10	704 699
P/2004 VR$_8$	JF	12.74	8.2	33	704 644 699 703 691
P/2004 WR$_9$	JF	16.42	1.5	12	649 673 704
C/2004 RG$_{113}$	DO	14.07	4.4	38	704
C/2004 K3	DO	18.20	0.7	37	854 926 649 673 704
C/2004 HV$_{60}$	HT	16.19	1.7	15	291 691
P/2004 EW$_{38}$	JF	16.48	1.5	23	704 699 703
C/2004 DZ$_{61}$	DO	15.30	2.5	112	854 926 649 673 704 644 A50 703
C/2004 D1	DN	10.59	21.4	9	926 704 644
P/2004 CB	JF	16.80	1.2	29	926 649 673 704
P/2004 DO$_{29}$	JF	13.06	6.9	26	704 699 703 691
P/2003 WC$_7$	JF	16.00	2.0	14	704 703
P/2003 SQ$_{215}$	JF	14.14	4.3	22	704 644 699 703
C/2003 WT$_{42}$	DN	8.84	48.7	69	854 926 673 704 291 691
P/2003 UY$_{275}$	JF	16.26	1.6	33	704 644
P/2003 QX$_{29}$	JF	12.97	7.2	7	673 644
C/2002 X1	DO	11.87	12.3	21	926 704 644
P/2002 LZ$_{11}$	JF	13.69	5.4	53	704 699 608
C/2002 V2	DO	9.92	30.7	24	926 649 704 608
C/2002 VQ$_{94}$	DO	8.65	52.8	66	926 649 704 644 711
P/2003 HT$_{15}$	JF	14.37	3.8	32	704 608
C/2002 T7	DN	8.68	52.0	23	854 926 649 704
P/2002 T6	JF	14.19	4.2	20	704 644
P/2002 T5	JF	11.89	11.9	17	704
C/2002 L9	DO	8.43	58.9	23	704 644

45

Table 3: Continued.

Comet	type	H(1,1,0)	R_N [km]	n	Observers
P/2002 JN$_{16}$	JF	15.84	1.9	47	704 644 608
C/2002 J5	DN	9.89	30.3	7	704 608
P/2002 EJ$_{57}$	JF	14.84	3.1	27	704 644
P/2002 AR$_2$	JF	15.43	2.3	26	704
C/2002 A2	JF	12.02	11.6	11	704 644
P/2002 CW$_{134}$	JF	16.34	1.6	23	704 608
P/2001 YX$_{127}$	JF	13.84	4.8	3	704
C/2002 B3	DN	10.95	18.3	25	649 704
C/2002 B2	DO	12.05	11.0	13	649 704
C/2001 OG$_{108}$	HT	12.88	7.5	24	649 644 699 608
P/2001 TU$_{80}$	JF	14.79	3.2	3	608
C/2001 RX$_{14}$	DN	10.81	19.4	12	644 699
C/2001 G1	DN	7.86	76.1	5	699 608
C/2001 A2	DO	14.55	3.5	1	699
C/2000 SV$_{74}$	DN	9.33	38.5	7	649 699
C/2000 OF$_8$	DN	14.18	4.1	13	691
P/1999 XN$_{120}$	JF	12.57	9.1	14	699 703
P/1998 VS$_{24}$	JF	13.38	5.9	2	699
P/1998 QP$_{54}$	JF	15.09	2.7	3	699
183P	JF	12.11	10.6	2	699
182P	JF	18.91	0.6	13	704 699 608
172P	JF	14.10	4.4	33	704 691
169P	JF	15.80	2.0	39	704 644 A50 691
167P	CT	9.27	40.1	23	673 644 291
162P	JF	13.81	5.0	38	704 644 699 I05 608
160P	JF	15.51	2.3	39	704 699 691
159P	JF	13.44	5.9	21	704 644 699 703
158P	JF	12.06	11.2	41	704 644 699 703 608
150P	JF	13.50	5.6	13	854 699 608
148P	JF	15.08	2.8	3	699
139P	JF	12.72	8.0	1	699

Table 4: Values for r_{min} and α when fitting only to nuclear radii larger than r_{limit}, for the different data sets analyzed in this work. The results for the compilation of nuclear radii from the literature are computed assuming σ to be independent of the radius. n gives the number of comets included in the fits, and P_{KS} the level of confidence according to a KS-test.

r_{limit} [km]	r_{min} [km]	α	n	P_{KS}
Jupiter Family				
0.0	$1.55^{+0.22}_{-0.20}$	$2.01^{+0.21}_{-0.17}$	46	0.114
2.0	$3.38^{+0.50}_{-0.44}$	$2.76^{+0.54}_{-0.40}$	34	0.445
3.0	$4.64^{+0.69}_{-0.61}$	$3.6^{+1.1}_{-0.71}$	29	0.510
4.0	$5.80^{+0.83}_{-0.72}$	$4.6^{+2.2}_{-1.2}$	25	0.790
5.0	$7.36^{+1.05}_{-0.91}$	$7.4^{+10.7}_{-2.8}$	20	0.275
Isotropic comets				
0.0	$2.03^{+0.78}_{-0.67}$	$1.56^{+0.15}_{-0.12}$	37	0.033
5.0	$8.1^{+1.3}_{-1.1}$	$2.13^{+0.30}_{-0.24}$	28	0.515
10.0	$13.1^{+1.9}_{-1.7}$	$2.51^{+0.47}_{-0.37}$	22	0.705
15.0	$18.2^{+3.3}_{-2.7}$	$2.84^{+0.80}_{-0.54}$	17	0.846
20.0	$35.3^{+7.1}_{-6.3}$	$6.0^{+9.8}_{-2.5}$	11	0.000
Compilation of radii from literature				
0.0	$0.623^{+0.022}_{-0.025}$	$1.98^{+0.16}_{-0.14}$	46	
1.0	$1.087^{+0.028}_{-0.035}$	$2.32^{+0.25}_{-0.22}$	34	
2.0	$2.064^{+0.015}_{-0.042}$	$2.96^{+0.51}_{-0.43}$	18	*n.a.*
3.0	$3.142^{+0.018}_{-0.067}$	$4.0^{+1.0}_{-0.83}$	11	
4.0	$4.50^{+0.15}_{-0.23}$	$4.4^{+1.9}_{-1.4}$	5	

Table 5: Compilation of radii of Jupiter Family comets from the literature. The columns give the comet's name, the nuclear radius in km, the error of the radii in km, the reference, the method applied for determining the radii (coma sub. – subtraction of the coma contribution from the nuclear signal for active comets, distant – obseration of an inactive comet at large r_h, S/C – resolved imaging during a spacecraft flyby, thermal – analysis of thermal infrared observations), a flag whether the radius determination includes the effects of lightcurve variation (– no, + yes), and the value adopted in this work for the analysis of the size frequency distribution, in km.

Comet	R_N	σ	Reference	method	lc	adopted
4P/Faye	1.77	0.04	Lamy et al. (2009)	coma sub.	–	1.77 ± 0.04
6P/d'Arrest	1.52	0.05	Meech et al. (2004)	distant	–	1.64 ± 0.03
	1.71	0.04			–	
7P/Pons-Winnecke	2.24	0.02	Snodgrass et al. (2005)	distant	+	2.24 ± 0.02
	4.40	0.10	Lowry et al. (2001)	distant	–	
9P/Tempel 1	3.00	0.10	A'Hearn et al. (2005)	S/C	n.a.	3.00 ± 0.10
10P/Tempel 2	5.98	0.04	Lamy et al. (2009)	coma sub.	–	4.99 ± 0.02
	4.50	0.03	Meech et al. (2004)	distant	–	
	4.93	0.03			–	
14P/Wolf	3.16	0.01	Snodgrass et al. (2005)	distant	+	3.16 ± 0.01
	2.33	0.12	Lowry et al. (2003)	distant	–	
17P/Holmes	1.62	0.01	Snodgrass et al. (2006)	distant	–	1.62 ± 0.01
	1.71	0.07	Lamy et al. (2009)	coma sub.	–	
19P/Borrelly	1.90	0.32	Lowry et al. (2003)	distant	–	2.81 ± 0.24
	2.81	0.24	Lamy et al. (1998b)	coma sub.	+	
	1.89	0.16	Groussin et al. (2009)	thermal	–	
22P/Kopff	1.67	0.18	Lamy et al. (2002)	thermal	+	1.80 ± 0.08
	1.80	0.10	Lowry et al. (2001)	distant	–	
26P/Grigg-Skjellerup	1.44	0.05	Boehnhardt et al. (1999)	distant	+	1.44 ± 0.05
28P/Neujmin 1	10.83	0.25	Meech et al. (2004)	distant	–	11.29 ± 0.12
	11.44	0.14			–	
37P/Forbes	0.81	0.04	Lamy et al. (2009)	coma sub.	–	0.81 ± 0.04
43P/Wolf-Harrington	3.43	0.22	Lowry et al. (2003)	distant	–	3.43 ± 0.22
44P/Reinmuth 2	1.61	0.07	Lamy et al. (2009)	coma sub.	–	1.61 ± 0.07
45P/Honda-Mrkos-Pajdusakova	1.34	0.55	Lowry et al. (2003)	distant	–	1.34 ± 0.55
	0.34	0.01	Lamy et al. (1999)	coma sub.	–	
46P/Wirtanen	0.62	0.02	Lamy et al. (1998a)	coma sub.	+	0.62 ± 0.02
47P/Ashbrook-Jackson	3.38	0.01	Snodgrass et al. (2006)	distant	–	3.38 ± 0.01
49P/Arend-Rigaux	4.60	0.11	Lowry et al. (2003)	distant	–	4.60 ± 0.11
50P/Arend	0.95	0.03	Lamy et al. (2009)	coma sub.	–	0.95 ± 0.03
53P/van Biesbroeck	3.37	0.09	Meech et al. (2004)	distant	–	3.35 ± 0.06
	3.33	0.09			–	
56P/Slaughter-Burnham	1.56	0.09	Meech et al. (2004)	distant	–	1.56 ± 0.09
59P/Kearns-Kwee	0.79	0.03	Lamy et al. (2009)	coma sub.	–	0.79 ± 0.03
61P/Shajn-Schaldach	0.92	0.24	Lowry et al. (2003)	distant	–	0.92 ± 0.24
63P/Wild 1	1.46	0.03	Lamy et al. (2009)	coma sub.	–	1.46 ± 0.03
67P/Churyumov-Gerasimenko	1.87	0.08	Kelley et al. (2008)	thermal	–	1.98 ± 0.05
	1.98	0.05	Lamy et al. (2008)	thermal	+	
69P/Taylor	3.60	0.70	Lowry et al. (1999)	distant	–	3.60 ± 0.70
71P/Clark	0.68	0.04	Lamy et al. (2009)	coma sub.	–	1.00 ± 0.03
	1.31	0.04	Meech et al. (2004)	distant	–	
73P/Schwassmann-Wachmann 3	1.10	0.03	Boehnhardt et al. (1999)	distant	+	1.10 ± 0.03
79P/du Toit-Hartley	1.40	0.30	Lowry et al. (1999)	distant	–	1.40 ± 0.30
81P/Wild 2	2.09	0.01	Brownlee et al. (2004)	S/C	n.a.	2.09 ± 0.01
84P/Giclas	0.90	0.05	Lamy et al. (2009)	coma sub.	–	0.90 ± 0.05
86P/Wild 3	1.10	0.20	Lowry et al. (1999)	distant	–	0.68 ± 0.02
	0.73	0.04	Meech et al. (2004)	distant	–	
	0.65	0.03			–	

48

Table 5: Continued.

Comet	R_N	σ	Reference	method	lc	adopted
92P/Sanguin	2.08	0.01	Snodgrass et al. (2005)	distant	+	2.08 ± 0.01
	1.19	0.20	Meech et al. (2004)	distant	−	
97P/Metcalf-Brewington	2.18	0.41	Lowry et al. (2003)	distant	−	2.18 ± 0.42
103P/Hartley 2	0.57	0.08	Lisse et al. (2009)	thermal	−	0.57 ± 0.08
	0.71	0.13	Groussin et al. (2004)	thermal	−	
104P/Kowal 2	1.04	0.46	Lowry et al. (2003)	distant	−	1.04 ± 0.46
106P/Schuster	0.94	0.03	Lamy et al. (2009)	coma sub.	−	0.94 ± 0.03
112P/Urata-Niijima	0.90	0.05	Lamy et al. (2009)	coma sub.	−	0.90 ± 0.05
114P/Wiseman-Skiff	0.78	0.05	Lamy et al. (2009)	coma sub.	−	0.78 ± 0.05
115P/Maury	1.11	0.03	Meech et al. (2004)	distant	−	1.11 ± 0.03
118P/Shoemaker-Levy 4	2.42	0.22	Lowry et al. (2003)	distant	−	2.42 ± 0.22
120P/Mueller 1	1.50	0.20	Lowry et al. (1999)	distant	−	1.50 ± 0.20
121P/Shoemaker-Holt 2	1.62	0.57	Lowry et al. (2003)	distant	−	1.62 ± 0.57
137P/Shoemaker-Levy 2	3.38	0.05	Snodgrass et al. (2003)	distant	−	3.38 ± 0.05
143P/Kowal-Mrkos	5.70	0.60	Jewitt et al. (2003)	distant	+	5.70 ± 0.60
162P/Siding Spring	6.00	0.80	Fernandez et al. (2006)	thermal	−	6.00 ± 0.80

−We determine cometary nuclear magnitudes from sky survey observations
−We present a method to derive size frequency distributions from sparse noise power law data
−We derive size frequency distributions for Jupiter Family comets and isotropic comets
−The size frequency distribution of isotropic comets is shallower than for Jupiter Family comets